SPIE. FIELD GUIDE

Field Guide to Fiber Optic Sensors

William B. Spillman, Jr.
Eric Udd

Field Guide to

Fiber Optic Sensors

William B. Spillman, Jr.
Eric Udd

SPIE Field Guides
Volume FG34

John E. Greivenkamp, Series Editor

SPIE PRESS
Bellingham, Washington USA

Library of Congress Preassigned Control Number Data

Spillman, William B., author.
Field Guide to Fiber Optic Sensors / William B. Spillman, Jr. and Eric Udd
pages cm. – (The field guide series; FG34)
Includes bibliographical references and index.
ISBN 978-1-62841-334-2
1. Fiber optics–Design and application. 2. Sensor design. I. Title.
TA1800 2014
681.2–dc23

2014954702

Published by

SPIE
P.O. Box 10
Bellingham, Washington 98227-0010 USA
Phone: 360.676.3290
Fax: 360.647.1445
Email: Books@spie.org
www.spie.org

Printed in the United States of America.
Last updated 02/10/2015

Introduction to the Series

Welcome to the *SPIE Field Guides*—a series of publications written directly for the practicing engineer or scientist. Many textbooks and professional reference books cover optical principles and techniques in depth. The aim of the *SPIE Field Guides* is to distill this information, providing readers with a handy desk or briefcase reference that provides basic, essential information about optical principles, techniques, or phenomena, including definitions and descriptions, key equations, illustrations, application examples, design considerations, and additional resources. A significant effort will be made to provide a consistent notation and style between volumes in the series.

Each *SPIE Field Guide* addresses a major field of optical science and technology. The concept of these *Field Guides* is a format-intensive presentation based on figures and equations supplemented by concise explanations. In most cases, this modular approach places a single topic on a page, and provides full coverage of that topic on that page. Highlights, insights, and rules of thumb are displayed in sidebars to the main text. The appendices at the end of each *Field Guide* provide additional information such as related material outside the main scope of the volume, key mathematical relationships, and alternative methods. While complete in their coverage, the concise presentation may not be appropriate for those new to the field.

The *SPIE Field Guides* are intended to be living documents. The modular page-based presentation format allows them to be updated and expanded. We are interested in your suggestions for new *Field Guide* topics as well as what material should be added to an individual volume to make these *Field Guides* more useful to you. Please contact us at **fieldguides@SPIE.org**.

John E. Greivenkamp, *Series Editor*
College of Optical Sciences
The University of Arizona

The Field Guide Series

Keep information at your fingertips with the SPIE Field Guides:

Adaptive Optics, Second Edition, Robert Tyson & Benjamin Frazier

Atmospheric Optics, Larry Andrews

Binoculars and Scopes, Paul Yoder, Jr. & Daniel Vukobratovich

Diffractive Optics, Yakov Soskind

Digital Micro-Optics, Bernard Kress

Displacement Measuring Interferometry, Jonathan Ellis

Fiber Optic Sensors, William Spillman, Jr. & Eric Udd

Geometrical Optics, John Greivenkamp

Holography, Pierre-Alexandre Blanche

Illumination, Angelo Arecchi, Tahar Messadi, & John Koshel

Image Processing, Khan M. Iftekharuddin & Abdul Awwal

Infrared Systems, Detectors, and FPAs, Second Edition, Arnold Daniels

Interferometric Optical Testing, Eric Goodwin & Jim Wyant

Laser Pulse Generation, Rüdiger Paschotta

Lasers, Rüdiger Paschotta

Lens Design, Julie Bentley & Craig Olson

Microscopy, Tomasz Tkaczyk

Nonlinear Optics, Peter Powers

Optical Fabrication, Ray Williamson

Optical Fiber Technology, Rüdiger Paschotta

Optical Lithography, Chris Mack

Optical Thin Films, Ronald Willey

Optomechanical Design and Analysis, Katie Schwertz & James Burge

Physical Optics, Daniel Smith

Polarization, Edward Collett

Probability, Random Processes, and Random Data Analysis, Larry Andrews

Radiometry, Barbara Grant

Special Functions for Engineers, Larry Andrews

Spectroscopy, David Ball

Terahertz Sources, Detectors, and Optics, Créidhe O'Sullivan & J. Anthony Murphy

Visual and Ophthalmic Optics, Jim Schwiegerling

Fiber optic sensor work began in the mid-1970s with a variety of multimode fiber optic sensors and early iterations of Sagnac and Mach–Zehnder interferometers. Concerted efforts developed fiber optic gyros and acoustics sensors in the form of hydrophones; fiber gyros are currently used for aircraft and spacecraft navigation, including the Spirit and Opportunity rovers on Mars. They are used for naval and land navigation, in robots that mow soccer fields and clean floors, and in remote-controlled helicopters that spray crops. Acoustic technology originally developed for undersea surveillance is now used to support oil and gas exploration and extraction operations.

In the mid-1980s the field of fiber optic smart structures emerged as a way to monitor the health and integrity of structures through the manufacturing process, during installation, and throughout the lifetime of the structure. Distributed sensors based on Raman and Brillouin scattering have been used to support cure monitoring on large concrete structures such as dams and to monitor oil holes and pipelines.

The continued improvement and reduction in costs associated with fiber optic technology associated with fiber sensors permit application areas that were previously inaccessible. These trends are expected to continue as new techniques become available and older ones are successfully adapted to new applications.

This Field Guide provides a broad introduction to a variety of fiber optic sensors that have been successfully developed from the 1970s to the present. We hope that the included examples inspire readers with ideas for new sensors and applications.

William B. Spillman, Jr.
Floyd, Virginia

Eric Udd
Fairview, Oregon

Table of Contents

Table of Contents

Table of Contents

Table of Contents

Glossary

a	Fiber core radius
A	Amplitude or some constant value
APD	Avalanche photodiode
B	Bandwidth
$\mathbf{B}$	Magnetic flux vector
c	Speed of propagation of an electromagnetic wave
c_e	Effective speed of light
d	Grating period, Bragg grating period, or lateral misalignment
d_0, d_1	Chirped grating parameters
D_i	Distance from a photodetector to the i^{th} element
d_{ij}	Distance between optical elements i and j
e	Electric charge or base of natural logarithms
$\mathbf{E}$	Electric-field vector
EH	Hybrid mode with more electric field than magnetic field $\perp$ to the direction of propagation
f	Frequency (in Hertz), or the lens focal length
F	Finesse
F	Power emitted by a blackbody
FBG	Fiber Bragg grating
f_D	Disk rotation frequency
FDM	Frequency division multiplexing
f_M	Modulation frequency
FTIR	Frustrated total internal reflection
f_σ	Material stress-optic coefficient
Ge	Germanium
GRIN	Graded index
h	Height
h	Planck's constant
HE	Hybrid mode with more magnetic field than electric field $\perp$ to the direction of propagation
He-Ne	Helium-neon
I	Optical power
i_0	Reverse "dark current"
I_B	Background optical power
I_d	Dark current
i_s	Photocurrent
$\mathbf{k}$	Wave vector

Glossary

k_B	Boltzman's constant
L	Length of a GRIN lens
LED	Light-emitting diode
m	Diffraction order
n	Index of refraction
N	Number of slots around a disk edge, or number of excited electrons
NA	Optical-fiber numerical aperture
n_{eff}	Effective index of refraction
OD	Optical density
OFDR	Optical frequency domain reflectometry
OTDR	Optical time domain reflectometry
p	Pitch of a GRIN lens
P	Pressure or detected optical power
PD	Photodiode
P_e	Photoelastic constant
P_{min}	Minimum detectable acoustic pressure
PVF	Polyvinyl fluoride
r	$\perp$ distance from optical axis
$\mathbf{r}$	Position vector
R	Electrical resistance or responsivity
R	Reflectivity
R_E, R_T	Fluorescent decay constants
RGB	Red–green–blue
R_p	p-polarized intensity reflectivity
R_s	s-polarized intensity reflectivity
s	Optical fiber longitudinal misalignment
s_1	Distance of an object from the center of a lens
s_2	Distance of an image from the center of a lens
S_n	Fluorescent signal level
SNR	Signal-to-noise ratio
t	Time
T	Absolute temperature
T_A	Fiber axial displacement fractional transmission
TDM	Time division multiplexing
TE	Mode with an electric field $\perp$ to the direction of propagation
TEM	Mode with both magnetic and electric fields $\perp$ to the direction of propagation

Glossary

T_i	Transducer function
TIR	Total internal reflection
T_L	Fiber longitudinal fractional transmission
TM	Mode with magnetic field ⊥ to the direction of propagation
UV	Ultraviolet
V	V-number, or voltage
V_B	Reverse bias voltage
VOD	Velocity of detonation
V_R	Voltage from a reference photodetector
W	Watts
WDM	Wavelength division multiplexing
z	FTIR variable
α	Fractional transmission factor, fluorescent decay probability, or thermal expansion coefficient
α_m	Angle of the m^{th} diffraction order
β	Mode-propagation constant, or FTIR variable
ΔE	Energy-level difference in fluorescent decay
ε	Dielectric permittivity, or mechanical strain
ζ	Thermo-optic coefficient
η	Quantum efficiency
θ	Angle
θ_D	Angle of diffraction
λ	Wavelength
λ_B	Wavelength Bragg grating maximum reflection
Λ	Microbend optimum deformer spacing
μ	Magnetic susceptibility
μW	Microwatts
σ	Linear stress
τ	e^{-1} fluorescent decay time
ϕ	Phase
ω	Angular frequency in radians/sec

What Is a Fiber Optic Sensor?

A **fiber optic sensor** is a device that uses a transducer to map a parameter or parameters of interest onto one or more of the properties of the light propagating in an optical fiber. The light is then detected and analyzed at a signal-processing location where the values of the parameter/s of interest are extracted from the optical signal. A schematic diagram of a fiber optic sensor is shown below, where the transducer can be either the fiber or some arrangement of external optics.

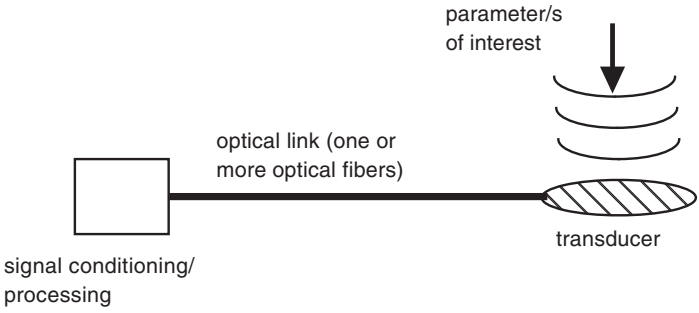

Optical fibers are very thin strands of extremely-low-loss glass (or higher-loss plastic) that act as essentially lossless waveguides for light. They generally consist of an inner core of material that has a lower speed of light (higher refractive index) than that of the surrounding cladding. From the standpoint of geometrical optics, light is confined to the core via total internal reflection. **Multimode optical fibers** allow many optical paths, whereas **single-mode optical fibers** allow only one.

An **extrinsic fiber optic sensor** is one in which the light is removed from the optical fiber, acted upon by the transducer, and then coupled back into the same fiber or a separate fiber. An example of this type of sensor is the Schlieren fiber optic hydrophone.

An **intrinsic fiber optic sensor** is one in which the light in the fiber is acted upon by the transducer without leaving the fiber. An example of this type of sensor is the Mach–Zehnder interferometric hydrophone.

Why Use a Fiber Optic Sensor?

The first fiber optic sensor was the **endoscope**, followed by the **proximity** sensor in the 1960s. In the late 1970s fiber sensors were developed as alternative methods of sensing acoustic signals in the ocean (replacing piezoceramic hydrophones) and rotation rate (replacing mechanical gyroscopes). Since that time, fiber optic sensors have been developed for almost every sensing application.

The advantages of fiber optic sensors include light weight, small size, electrically passive transduction, low power requirements, resistance to electromagnetic interference, high sensitivity, wide bandwidth, and environmental ruggedness, among others.

In addition to being able to provide higher performance than many existing sensors, fiber optic sensing has greatly benefited from the maturation of the fiber optic telecommunications industry. Mass production and process refinements in that field have resulted in significant cost reductions for components that are part of any fiber optic sensor system. This is particularly true for optical fiber, LED, and laser diode sources, optical detectors, fiber optic splitters, fiber optic connectors, and various other passive and active optical components.

The following questions are also relevant and can be used in cost–benefit analysis to determine whether a fiber optic sensor is the best fit for an application:

1. What is being measured, how well, and under what conditions (the specification)?
2. What optical transducer mechanism will best convert changes in the parameter/s into changes in the properties of light traveling through a fiber?
3. What optical fiber is required?
4. What optical source is needed?
5. Which optical detector must be used?
6. What optical source/detector signal conditioning is required?

Light as an Electromagnetic Wave

A triumph of classical physics occurred when **Maxwell's equations** unified electricity and magnetism and implied the existence of **electromagnetic waves** that were soon shown to be identical with visible light, which in a vacuum has an electrical component **E** and a magnetic component **B**, which are orthogonal to each other and to the direction of propagation **k**. The wave equation in terms of the electrical component is

$$\nabla^2 \mathbf{E}(\mathbf{r}, t) = \left(\frac{1}{c^2}\right) \frac{\partial^2}{\partial t^2} \mathbf{E}(\mathbf{r}, t)$$

where c is the speed of propagation, t is the time, and **r** is the position in space. The speed of the wave is related to the medium of propagation according to

$$c = \frac{1}{\sqrt{\mu\varepsilon}}$$

where ε is the dielectric permittivity, and μ is the magnetic susceptibility of the medium. The solution to the wave equation in a vacuum is a **plane wave**:

$$\mathbf{E}(\mathbf{r}, t) = \mathrm{Re}\{\mathbf{E}_0 \exp[i(\omega t - \mathbf{k} \cdot \mathbf{r} + \phi_0)]\}$$

In this case, ω is the angular frequency, and **k** is the wave vector pointing in the direction of wave propagation. The wave vector is related to other wave parameters according to

$$k = |\mathbf{k}| = \frac{\omega}{c} = \frac{2\pi}{\lambda}$$

where λ is the wavelength of the light, as shown below.

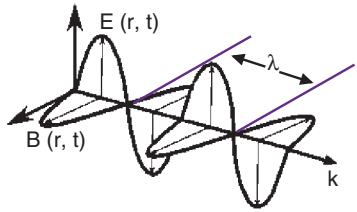

Light Modulation

Light has a number of properties that can be **modulated** via various physical mechanisms. However, it should be noted that for a fiber optic sensor, no matter what physical processes take place, the last step always involves converting light into an electrical current. How that electrical current relates to the parameter of interest depends on the physical configuration of the sensor, optical light source, and optical detector.

The solution to the electromagnetic wave equation contains the **properties of light** that can be modulated:

- the speed of light c,
- the direction of the light (along the $\mathbf{k}$ vector),
- the frequency of the light f ($2\pi f = \omega$),
- the phase of the light ϕ,
- the wavelength of the light λ (color),
- the polarization of the light (along the direction of the electric field vector $\mathbf{E}$), and
- the intensity of the light I (proportional to the light's electrical field squared $\mathbf{E} \cdot \mathbf{E}$)

The approximate working ranges of these parameters are

- the speed of light between 3×10^8 m/s (air, vacuum) and 1.2×10^8 m/s (diamond) (for optical fibers, $c = \sim 2.1 \times 10^8$ m/s),
- the direction of the $\mathbf{k}$ vector, which in spherical coordinates can range from 0–2π in θ and 0–π in ϕ, where ϕ is not the same angle as the optical phase,
- the frequency of light can range from 1.9×10^{14} Hz (near infrared) to 7.5×10^{14} Hz (near ultraviolet),
- the effective phase of the light can range from 0–2π,
- the wavelength of light ranges from 0.4–1.6 μm,
- the direction of polarization of the light can range from 0–2π in the plane perpendicular to $\mathbf{k}$, and
- typical light intensities range from 0 to tens of milliwatts.

In practice, it should be noted that due to the extremely high frequency of light, simple linear polarization measurements treat polarization at θ and $\theta + \pi$ as equal.

Optical Signal-to-Noise Ratio

One of the defining characteristics of an optical sensor is the **signal-to-noise ratio** (SNR). Knowledge of this parameter allows one to determine the minimum detectable change in the optical signal and thus that of the parameter of interest. The variables involved can be seen in an analysis of a photodiode detector in **photoconductive mode**, shown below.

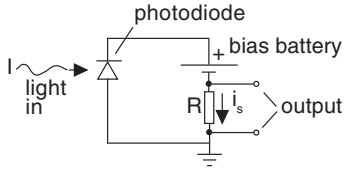

In this case, both the optical power I, representing the signal, and the background optical power I_B strike the photodiode, creating a photocurrent i_s in the load resistor R. The efficiency with which the photodiode coverts photons of light into electrons (electrical current) is η, and there is also a dark current i_d that passes through the photodiode even in the absence of light. For measurements made with a bandwidth B, the SNR is given by

$$SNR = \frac{2(Ie\eta/hf)^2}{\left[3e^2(I+I_B)\eta B/hf\right] + 2ei_dB + (4k_BTB/R)}$$

In this equation, e is the electronic charge, h is Planck's constant, K_B is Boltzman's constant, T is the absolute temperature in kelvins, and R is the load resistance in the detection circuit. The numerator represents the signal power and the three terms in the denominator represent **shot noise**, **dark-current noise**, and **thermal (Johnson) noise**, respectively. The minimum detectable optical power ($SNR = 1$) is

$$I_{\min} = \frac{hf}{e\eta}\sqrt{\frac{2k_BTB}{R}}$$

Transduction

A transducer is a physical mechanism that maps one parameter onto another, a process that is called **transduction**. These maps (**calibration curves**) can be thought of as simple graphs, as shown below.

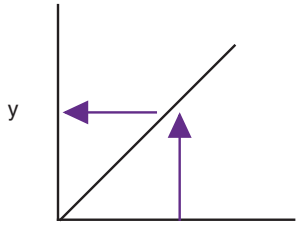

This graph represents a transducer that maps x onto y, or T(y, x).

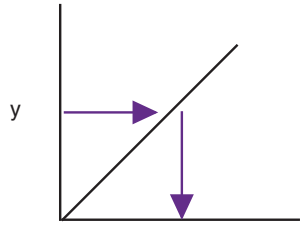

This graph is the inverse, mapping y onto x, or $T^{-1}(y, x)$.

Transducers often function in a serial manner. Consider how to determine the pressure P on a diaphragm that sits upon an optical fiber that is one arm of a Mach–Zehnder interferometer. First, the pressure maps onto the strain ε created in the fiber, or

$$\varepsilon = T_1(\varepsilon, P)P$$

The strain on the fiber maps onto the phase ϕ of light traveling through the fiber, i.e.,

$$\phi = T_2(\phi, \varepsilon)\varepsilon$$

The phase in the fiber maps onto the detected output intensity I from the Mach–Zehnder interferometer according to

$$I = T_3(I, \phi)\phi$$

Putting all the intermediate steps together,

$$I = T_3(I, \phi)T_2(\phi, \varepsilon)T_1(\varepsilon, P)P$$

This inversion of the final equation provides P as a function of I.

Some Optical Transducer Mechanisms

Perhaps the simplest fiber optic transduction mechanism is that of **optical absorption**. In this case, a parameter of interest modulates the absorption constants of the light-propagation medium. Light is attenuated by the medium, thereby mapping the value of the parameter of interest onto the light intensity.

The most common methods of modifying the properties of light in fiber optic sensors involve the **strain-optic effect**. When the medium of light propagation is strained, two things occur: first, the optical path length is changed by the strain. Second, the speed of light c (or index of refraction n) is also changed. Strain modulation can be used to affect the phase of the light ϕ, light direction through reflection and refraction, modal distribution, and other properties.

The **electro-optic effect** is another mechanism by which the properties of light can be modulated. In the Pockels or linear electro-optic effect, the refractive index of certain crystalline materials varies linearly with the electric field, producing field-dependent birefringence in the material. The electro-optic effect can be useful in both fiber optic sensors and modulators.

The properties of light can also be affected by the **magneto-optic effect**. When a magnetic field is applied to a magneto-optic material, the polarization of light traveling through the material rotates by an amount proportional to the applied magnetic field and the optical path length. Both fiber optic sensors and modulators can be based on this effect.

These are only a few of the different transducer mechanisms used in fiber optic sensors. Others include the **Sagnac effect** for rotation sensing and **blackbody radiation** detection and **fluorescence decay** for temperature sensing. (Detailed descriptions of fiber optic sensors and transducers are presented later.)

Optical Fibers and Modes

Optical fibers are thin and flexible structured cylinders made from glass so pure that the fibers are a lossless transmission medium for light of an appropriate wavelength λ and for sufficiently short distances. The simplest form of an optical fiber is the **step-index fiber**, in which a core glass with an index of refraction n_1 is surrounded by a cladding glass of index n_2, where $n_1 > n_2$. Light is confined to the fiber via the process of **total internal reflection** (TIR), i.e., a beam of light is totally reflected when it impinges from the n_1 side of a boundary between n_1 and n_2 regions if the angle of incidence $\theta > \sin^{-1}(n_2 / n_1)$.

The propagating light solutions of Maxwell's equations for a step-index fiber identify distinct wave configurations or **modes** that can propagate in the fiber. The lowest-order allowed modes are shown below.

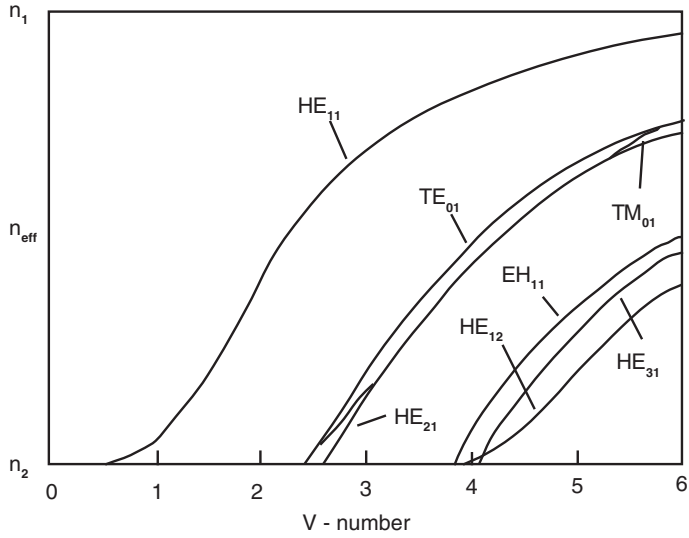

In this figure, the effective-mode index of refraction is $n_{\text{eff}} = (\beta\lambda/2\pi)$, the **V-number** is $V = (2\pi a/\lambda)\,(n_1^2 - n_2^2)^{1/2}$, the fiber core radius is a, and β is the mode-propagation constant. Note that this figure shows the allowed mode-propagation constants for a given core radius; for a V-number less than 2.405, only one mode can propagate.

Optical Fiber Types

All **optical fibers** are essentially configured in the same manner (see below), except for certain specialty fibers.

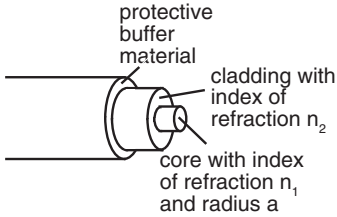

For any given fiber, a core of radius a and index of refraction n_1 is surrounded by a cladding of lower index of refraction n_2, which is in turn surrounded by a protective buffer coating. Individual fibers are identified as to whether they can support many or only one mode of propagation at an operational wavelength (i.e., $V < 2.405$ for **step-index fibers**). In addition to this general division into classes, the index of refraction in the core can be uniform as a function of radius, or, to reduce pulse dispersion, a fiber could have a **graded-index** profile in the core. The variation of index of refraction versus radius for a few of these situations is shown below.

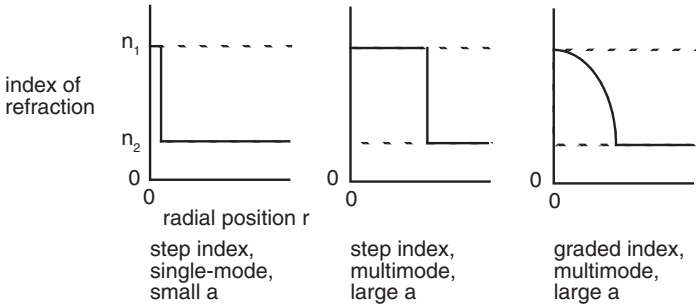

Additional optical fibers have been produced, including plastic optical fibers, glass optical fibers with plastic claddings, photonic crystal (holey) optical fibers, doped active optical fibers, and others.

Light-Emitting Diode

A **light-emitting diode** (LED) is a semiconductor device that produces light when a voltage forces a current through it. The device consists of two different types of semiconductor that are adjacent to each other.

- One side of the device, consisting of an **n-type semiconductor**, has an excess of electrons in its conduction band.
- The other side of the device, consisting of a **p-type semiconductor**, has a deficit of electrons (called holes) in its **valence band** (the energy band just below the conduction band).

When electrons from the n-type material are forced into the p-type material and holes from the n-type material are forced into the p-type material, some electrons from the conduction band fill some of the holes in the valence band. The excess energy, equal to the energy of the **bandgap**, is radiated as light.

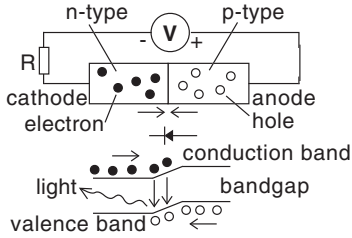

A typical optical output from an LED versus drive current is shown below.

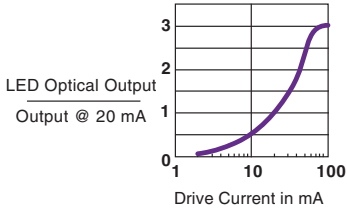

Semiconductor Laser Diode

When n-type and p-type semiconductor materials are abutted to each other, a **depletion region** forms around the junction due to the excess of holes in the p-type material combining with the charges in the n-type material. When a voltage is applied to the junction, this process dynamically continues, and a LED is the result. When the region is bounded by highly reflective end surfaces, the trapped photons stimulate additional electron–hole combination/photon creations, and lasing action ensues. A diagram of a simple **semiconductor laser diode** is shown below.

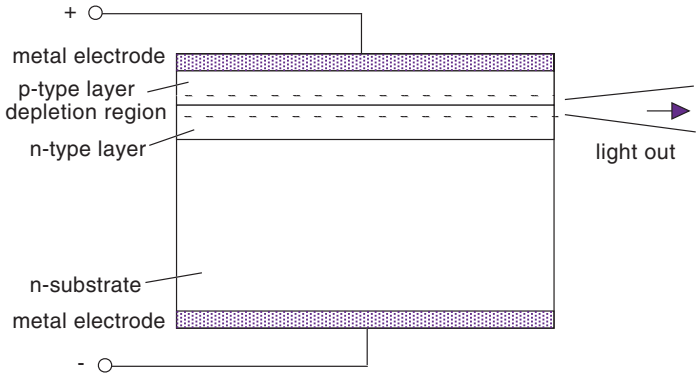

There are many other elaborations of the basic semiconductor laser scheme. In the **double heterostructure laser**, two high-bandgap layers contain a low-bandgap layer between them. These devices, in addition to having highly reflective end surfaces, reflect light in the central layer from the interfaces and effectively contain it to the middle region, making this type of semiconductor laser diode very efficient.

Other types of lasers:

- **quantum well lasers**, whose sharp cutoff in the density of states increases optical confinement,
- **distributed feedback lasers** that use an integral grating filter to create optical feedback into the active region for lasing, and
- **vertical-cavity surface-emitting lasers**, whose optical output is normal to the device plane rather than from its edge.

Photodiode Detector

A **photodiode optical detector** converts light into either voltage or current. The most common types consist of either a **p-n junction** (p-type semiconductor material abutted against n-type semiconductor material) or a **p-i-n junction**, in which a relatively wide layer of intrinsic semiconductor with a low level of doping is placed between the p- and n-type layers. In both configurations, photons are absorbed in a **depletion region** (around the junction in p-n devices or mostly within the **intrinsic region** for p-i-n devices), creating an electron–hole pair with local fields that sweep the electron into the n-type region and the hole into the p-type region, thereby creating a current. The typical **responsivity** R (amperes/watt) of the electrical current produced when an optical signal (with intensity measured in watts) is incident on a typical silicon photodiode detector is shown below.

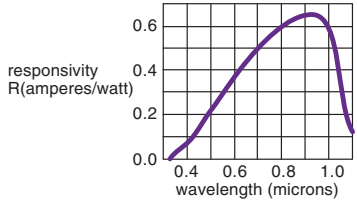

In the device's **photovoltaic mode**, no bias voltage is applied. If $A = e / k_B T$, where e is the electronic charge, k_B is Boltzman's constant, and T is the absolute temperature (with i_0 a reverse "dark current" and I the incident optical power), then the output voltage V across the device is given by

$$V \cong A \ln\left(R \frac{I}{i_0}\right)$$

In the device's **photoconductive mode**, a reverse bias V_B is applied, and the photocurrent i varies linearly with optical power:

$$i = i_0[\exp[(AV_B - 1)] - RI]$$

Avalanche Photodiode Detector

The **avalanche photodiode** is similar in construction to a p-i-n photodiode; the principal difference is that the depletion layer in the former is much thinner than the equivalent layer in the latter. When a high reverse-bias voltage is applied to the device, the electrons in the p-layer gain energy so that when a photon is absorbed, the electron promoted to the conduction band creates an "avalanche" of electrons instead of just one, as in the p-i-n photodiode case.

Avalanche photodiodes can be thought of as the solid state equivalent of the **photomultiplier tube** (PMT), or alternatively as a photodiode with an integrated gain stage. **Gain** as a function of reverse-bias voltage V is shown below for a typical avalanche photodiode. These devices have considerable temperature dependence and often must be thermally stabilized for optimal operation.

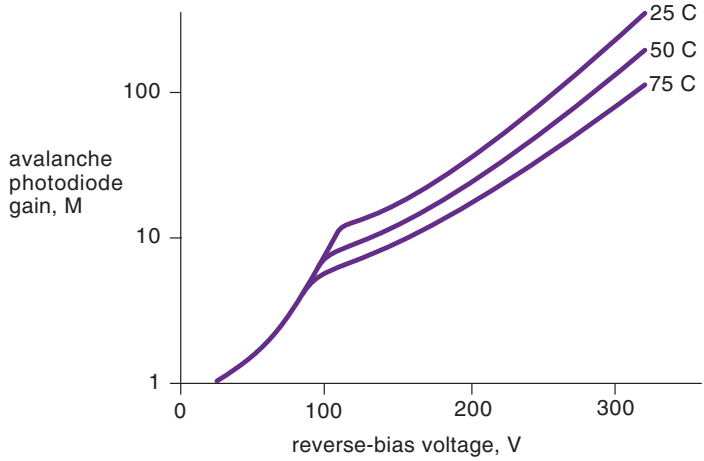

A simple operating circuit is shown below.

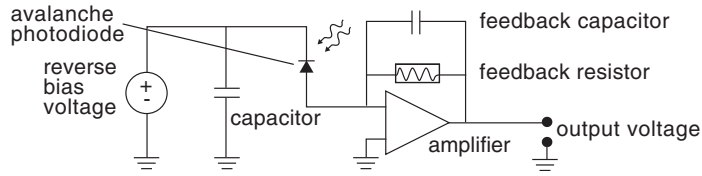

Color Sensors

The most common method of detecting the wavelength λ of a single **monochromatic signal** involves a spectrometer in which the optical signal is diffracted by a grating at different angles (depending on λ) and detected by either a photodiode array or a single fixed photodiode with a rotatable grating.

Other options include **RGB sensors**, in which three photodiodes have red, green, and blue filters in front of them. An interesting option for sensing wavelength and intensity of a single monochromatic sensor is the photodiode color sensor. When exposed to a monochromatic signal, this type of sensor, which has two stacked p-n junctions, provides two distinct outputs representing different responsivities in different regions of the photodiode. The region that is first encountered by the optical signal is more sensitive to red light [responsivity $R_1(\lambda)$], and the deeper region is more sensitive to blue light [responsivity $R_2(\lambda)$]. These responsivities for a typical device at room temperature are shown below.

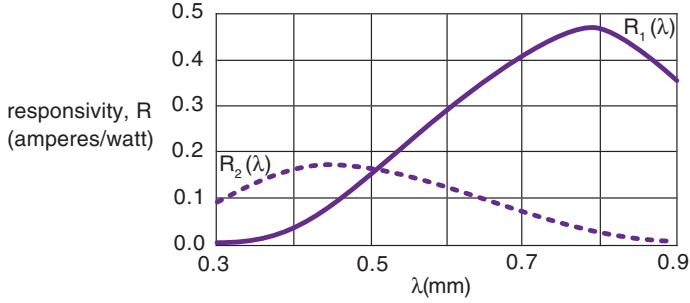

For any monochromatic signal within the region between ~0.45 mm and ~0.78 mm, the difference/sum of the two detected signals will be a monotonically increasing function, thereby allowing the signal's wavelength to be uniquely determined. However, the two detector responsivites are temperature dependent. This can be compensated for by using the diode as a temperature sensor, i.e., measuring some portion of the sensor's current–voltage curve in the absence of illumination, determining the temperature, and then adjusting the responsivities.

Connectors and Splices

Fiber optic **connectors** and **splices** serve the same purpose for the transmission of light (photons) as their electrical counterparts do for electricity (electrons). There are important differences, however. Mere contact between wires is usually sufficient to permit efficient electrical transmission, whereas optical fibers must be prepared with perfect end surfaces normal to the fiber axis, aligned coaxially, and pressed together surface to surface. Losses in optical fibers can occur when there is separation between the fiber end surfaces or axial or angular misalignment. Reflection and scattering from imperfections in the optical fiber end surfaces can also create losses.

Optical fiber connectors are used when fiber segments will need to be connected and disconnected repeatedly. There are a large number of different connector types on the market. A conceptual sketch of a basic fiber optic connector is shown below.

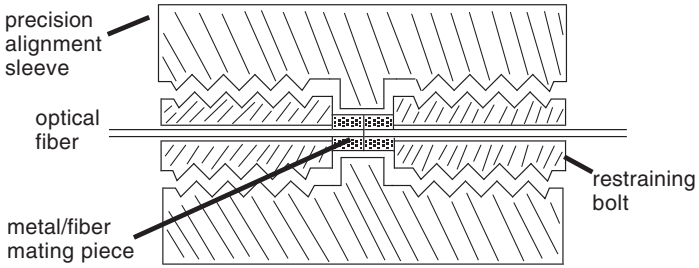

Optical fiber splices are connections that are considered to be effectively permanent. In this case, the fiber ends are prepared as in the connector case and then either fused under very high heat or butt coupled using a precision alignment sleeve or **v-groove** and secured in place using an optical bonding epoxy. A good splice will generally exhibit lower excess loss than a good connector.

Lenses and GRIN Lenses

Lenses are used to change the direction of light rays through refraction via **Snell's law**. A light ray encountering the boundary between one region with an index of refraction n_1 at an angle to the normal θ_1 will be refracted into an adjacent region of index n_2 at an angle to the normal θ_2 according to

$$n_1 \sin\theta_1 = n_2 \sin\theta_2$$

When $n_2 < n_1$, then total reflection back into region n_1 occurs when $\theta_1 = \sin^{-1}(n_2/n_1)$. A convex lens directs light encountering it parallel to the lens axis (through the center of the lens and normal to it) toward the lens axis. A concave lens directs light encountering it away from the lens axis. Lenses can form images of objects according to the **lensmaker's formula**. For a simple thin convex lens made of glass and surrounded by air, the formula is $(1/s_1) + (1/s_2) = (1/f)$, where s_1 is the distance of some object from the center of the lens along the lens axis, s_2 is the image distance, and f is the specified lens focal length. The image will be magnified by a factor of $-s_2/s_1$, where the minus sign indicates that the image will be inverted with respect to the object.

GRIN lenses are similar to graded-index optical fibers and have an index of refraction that varies with distance from the optical axis r according to $n = n_0\,(1 - Ar^2/2)$ where A is a constant. The pitch p of a GRIN lens is defined as $p = LA^{1/2}/2\pi$, where L is the length of the lens. The distance from the optical axis r_2 and its change of distance along the axis dr_2/dz of a ray exiting the lens in air when the ray entered the lens at r_1 and dr_1/dz is

$$\begin{pmatrix} r_2 \\ \dfrac{dr_2}{dz} \end{pmatrix} = \begin{bmatrix} \cos(2\pi p) & \dfrac{L}{2\pi n_0 p}\sin(2\pi p) \\ -\dfrac{2\pi n_0 p}{L}\sin(2\pi p) & \cos(2\pi p) \end{bmatrix} \begin{pmatrix} r_1 \\ \dfrac{dr_1}{dz} \end{pmatrix}$$

GRIN lenses can be used to minimize Fresnel reflection losses at the interfaces between different elements of optical systems.

Waveplates

The **polarization** of a light beam is the direction of the electric field associated with the beam. This polarization can be modified by passing it through an optical **waveplate**. A waveplate consists of a solid medium exhibiting **birefringence** that has two different indices of refraction depending on the polarization of the light entering it normal to its surface. Light that enters the waveplate with a polarization parallel to the **fast axis** (index $= n_2$) will have an apparent velocity in the plate faster than light polarized orthogonally along the **slow axis** (index $= n_1$). Light that is initially linearly polarized at an angle of $\pi/4$ to these two axes can be decomposed into two components that have an increasing **phase difference** ϕ as they progress a distance z into the waveplate. This change in phase is given by

$$\phi = 2\pi(n_2 - n_1)z/\lambda$$

where λ is the wavelength of the beam of light. The movement of the polarization vector of an incident light beam that is initially linear at $\pi/4$ to the fast and slow axes changes with increasing ϕ from linearly polarized to

- right elliptically polarized with the long axis at $\pi/4$,
- right circularly polarized,
- right elliptically polarized with the long axis at $3\pi/4$,
- linearly polarized at $3\pi/4$,
- left elliptically polarized with the long axis at $3\pi/4$,
- left circularly polarized,
- left elliptically polarized with the long axis at $\pi/4$, and
- linearly polarized along $\pi/4$.

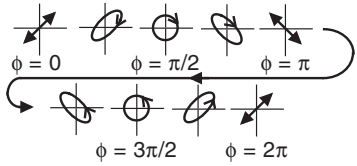

Some fiber optic sensors use parameter-dependent birefringence as a transducer mechanism.

Polarizers

Polarizers are optical elements whose effect on a light beam depends on the polarization or direction of the electric-field vector associated with that beam. It is important to note that due to the very high frequencies associated with light in or near the visible range (10^{14}–10^{15} Hz), the **instantaneous polarization** is hardly ever addressed by scientists, engineers, or device designers. Instead, they consider the shape traced out over time by the tip of the electric-field vector in a plane normal to the direction of the light beam.

The tip of the electric-field vector can trace out a straight line (**linear polarization**), an ellipse (right or left **elliptical polarization**), or a circle (right or left **circular polarization**). A polarizer will only transmit that particular polarization component for which it is designed.

When considering the aspects of polarization and the effects of polarizers, remember that the subject is a vector, not a scalar quantity. For example, assume that an unpolarized light beam of intensity I_0 encounters a linear polarizer with a transmission axis along θ_1. The light beam exiting the polarizer is linearly polarized along θ_1 with an intensity $I_0/2$. If this beam then encounters a second linear polarizer with a transmission axis along θ_2, then the light beam exiting the second polarizer will be polarized along θ_2 and have an intensity equal to $(I_0/2)\cos^2[\theta_1 - \theta_2]$. Next, assume that $(\theta_1 - \theta_2) = \pi/2$ radians so that no light is transmitted through the system. The vector nature of polarization can be seen when a third linear polarizer with a transmission axis along θ_3 is placed between the first two. When $\theta_3 =$ either θ_1 or θ_2, no light is transmitted through the system. However, when θ_3 has a different value from either of these, light will be transmitted, reaching a maximum when $\theta_3 = \pi/4$ radians.

Many fiber optic sensors incorporate polarization modulation within their transducer mechanisms.

Diffraction Gratings

A **diffraction grating** is a device that changes the propagation direction of a light beam by an angle that depends on the wavelength of the light. A typical grating consists of an array of parallel lines separated by spaces and can be configured in either a transmissive or reflective mode, or both. Gratings have been fabricated with complex surface topographies for specific applications, but the simplest grating consists of reflective lines interspersed with transmissive regions of equal width, as shown below.

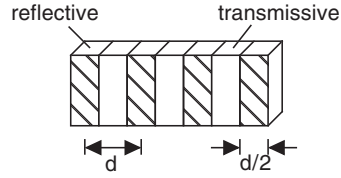

When a beam of light of wavelength λ is incident on this diffraction grating, the following situation results:

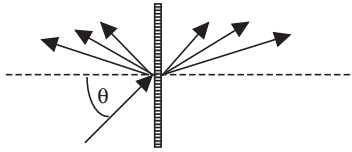

Output beams at different angles α_m result. This is described by the grating equation:

$$d(\sin\theta + \sin\alpha_m) = m\lambda \text{ or } \alpha_m = \sin^{-1}\left[\frac{m\lambda}{d} - \sin\theta\right]$$

Diffraction gratings have been used as the basis for the transducer mechanisms in some fiber optic sensors, but they are more generally used in spectrometers to demodulate the output from wavelength-modulating fiber optic sensors, such as those utilizing **fiber Bragg grating** (FBG) elements to convert parameters of interest to changes in the wavelength of reflected light.

Fiber Bragg Gratings

The Bragg formulation of x-ray diffraction is considered to be analogous to an optical plane wave of wavelength λ normally encountering a series of equivalent, partially reflecting mirrors, each separated by a distance d from adjacent mirrors. A peak in the amount of light reflected from this stack of mirrors will occur when the spacing of the mirrors is such that the light reflected from each mirror constructively interferes with the light reflected from all of the other mirrors. This is called satisfying the **Bragg condition**, or $2d = m\lambda$, where m is an integer.

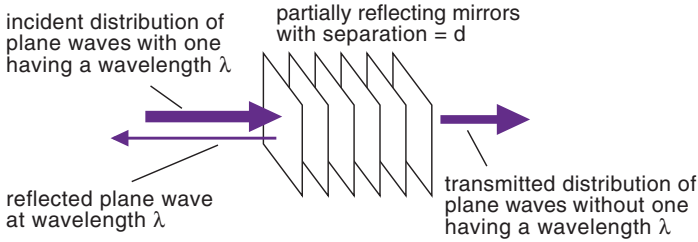

In a **fiber Bragg grating** (FBG), a periodic modulation (with period d) of the index of refraction of a single-mode optical fiber is introduced along its axis. This is essentially equivalent to the stack of partially reflecting mirrors considered in the x-ray diffraction analog; however, instead of a plane wave, there is a single propagating mode in the fiber. Light in an optical fiber travels slower than light in a vacuum, according to its effective index of refraction $n_e = c/c_e$, where c is the speed of light in a vacuum, and c_e is the effective speed of light of the propagating mode. The Bragg condition for an FBG then becomes $\lambda_B = 2n_e d$, where λ_B is the wavelength at which maximum reflection will occur.

FBGs are used as transducer mechanisms when they are configured so that some parameter of interest will modify n_e, d, or usually both. Various interrogation and compensation schemes can then be utilized to accurately extract the value of the parameter from the measured value of λ_B.

Modulators

Optical **modulators** are devices that change a property of light in a controllable manner. One of the most basic types of modulator is the **chopper**: a rotating disk with alternating slots around its outer edge. When a light beam is incident upon the edge, the intensity of the transmitted light is modulated (off and on) based on how fast the disk is rotating, the frequency f_D, and the number of slots around the disk edge N. The **intensity-modulation** frequency would then be $f_M = Nf_D$. Choppers are often used in laboratory situations to allow optical experimentation in ambient light conditions. A typical experiment analyzing an intensity-modulating fiber optic sensor is shown below.

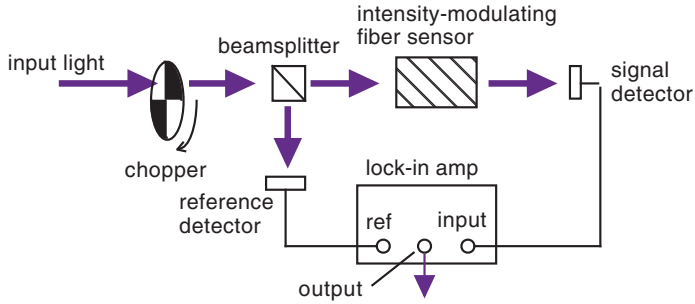

Other commonly used modulation methods include

- **direct modulation** of laser-diode or LED optical sources,
- **phase modulation** via strain, the electro-optic effect, or the magneto-optic effect, and
- **wavelength modulation** by modulating a laser diode's drive current.

Simple modulation of the phase via strain was used in the earliest Mach–Zehnder single-mode optical fiber hydrophones, as shown below.

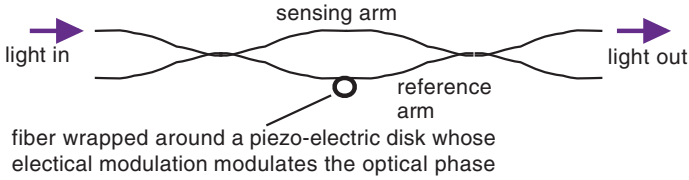

Specification and Transducer Selection

In order to design a fiber optic sensor for a particular application, one must first determine precisely what information is being sought. The different ways to obtain that information are considered (i.e., how much and what type of sensed data versus the amount of processing and estimation), and one way is selected. This selection then allows a **sensor specification** to be written that includes the dynamic range, sampling rate, accuracy, precision, environmental conditions, effective lifetime, maintenance, and (very importantly) cost. The sensor specification is compared to the available **optical transducer** mechanisms in a high-level **trade-off study** to identify the top candidates for incorporation into the sensor. These candidates are then analyzed by a detailed trade-off study, perhaps involving digital simulations, to choose the transducer to be used in the final design and development of the sensor.

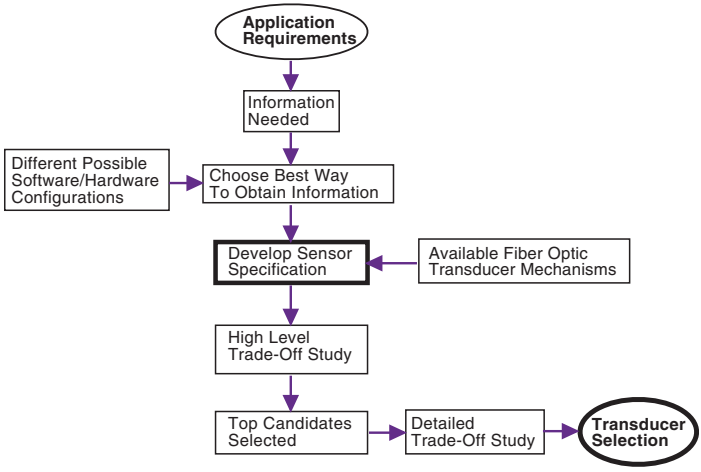

After the sensor specification has been completed and a transducer mechanism selected, the design of the sensor and its interfaces to the subsystems that are part of the overall system design can be initiated.

It cannot be emphasized enough that a sensor specification must precede all other aspects of sensor development.

Component Selection

The **selection of components** is driven by two factors: **cost** and **performance**. After the required information and the type of transducer are specified, based on the desired performance, the components can be identified by working backward from the fiber optic sensor output.

1. The required information will define the fiber sensor electrical output.
2. The sensor electrical output will determine the optical detection scheme and the optical signal delivered to the detector(s).
3. The delivered optical signal will determine the optical signal leaving the transducer based on the loss characteristics and length of the optical fiber used.
4. The optical signal leaving the transducer will determine the optical signal input to the transducer via the specific transducer characteristics.
5. The optical signal input to the transducer will determine the amount of optical power supplied to the input fiber from an optical source.

This analysis provides a way to approximately determine the characteristics of the optical detector(s) and associated electronics, the optical fiber characteristics, and the optical source characteristics.

There will generally be some number of detectors, fibers, and optical sources that meet all of these component specifications. **Optimization techniques** may then be used to create a specific collection of components that minimize sensor cost while simultaneously achieving (but not exceeding) the desired sensor performance.

Optimization techniques include **manual selection** in an ad hoc manner, **spreadsheet analysis** and **configuration trade-offs**, and more sophisticated optimization schemes, such as the **genetic algorithm**. Computer models of components developed can be used in sensor simulations.

Sensor Modeling

The development and availability of high-powered, cost-effective computers and software tools have changed the sensor-design process dramatically. In particular, it is now almost possible to develop designs directly from specifications. Human input can be minimal or considerable, depending on circumstances.

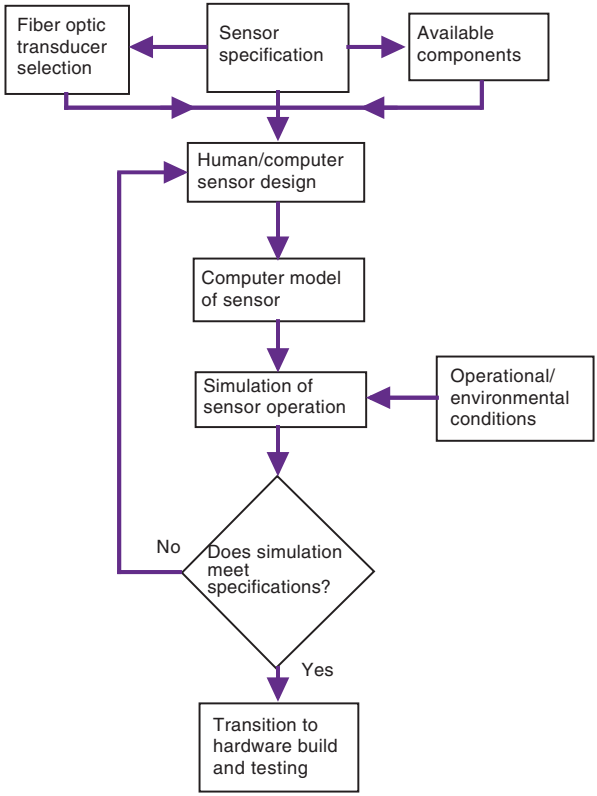

The advantage of following this kind of **design protocol** is primarily one of minimizing expensive hardware-design/environmental-testing iterations. It must be emphasized, however, that computer models and simulations are sometimes not perfect, and the building and testing of at least one prototype is necessary before proceeding to **final sensor development**.

FTIR Sensor Theory

When light traveling in a medium of index of refraction n_1 strikes the boundary of a medium of index of refraction n_2 at an angle θ_1, some fraction of the light will be transmitted across the boundary into medium 2 at an angle θ_2, according to **Snell's law**: $n_1 \sin\theta_1 = n_2 \sin\theta_2$, or $\sin\theta_2 = (n_1/n_2)\sin\theta_1$.

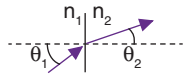

If $n_1 > n_2$, there is some angle θ_c for which $(n_1/n_2)\sin\theta_1$ (and, therefore, $\sin\theta_2$) must be greater than 1 and have an imaginary component. Physically, this means that no optical power is transmitted into medium 2. This phenomenon is called **total internal reflection** (TIR).

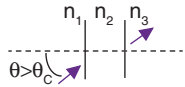

If a third medium is introduced, then it becomes **"frustrated" total internal reflection** (FTIR) due to electromagnetic "tunneling" from medium 1 to medium 3. In particular, if $n_1 = n_3 = n$, $n_2 = 1$, and a light beam of wavelength λ strikes the boundary between medium 1 and medium 2 at an angle $\theta > \theta_c$, then the fractional power T transmitted across the gap d from medium 1 to medium 3 will be given by

$$T = 1 - \left| (z^2 + \delta^2)^2 \left[(z^2 - \delta^2)^2 + 4z^2\delta^2 \coth^2 \beta \right]^{-1} \right|$$

where $\beta = (2\pi d/\lambda)(n^2\sin^2\theta - 1)^{1/2}$. For light polarized perpendicular to the plane of incidence,

$$z = 1/(n\cos\theta) \text{ and } \delta = -(n^2\sin^2\theta - 1)^{-1/2}$$

whereas for light polarized in the plane of incidence,

$$z = (\cos\theta)/n \text{ and } \delta = (n^2\sin^2\theta - 1)^{1/2}$$

FTIR Hydrophone

The first use of FTIR as the transducer mechanism in a fiber optic **hydrophone** occurred in 1980. Multimode optical fibers are polished optically flat at an angle of 76 deg to the multimode fiber axis to ensure that all modes propagating in the fiber will experience TIR upon reaching the polished fiber end. Two of these fiber ends are placed in close proximity in a hydrophone in which diaphragm displacements are used to modulate the gap between the two polished fiber ends.

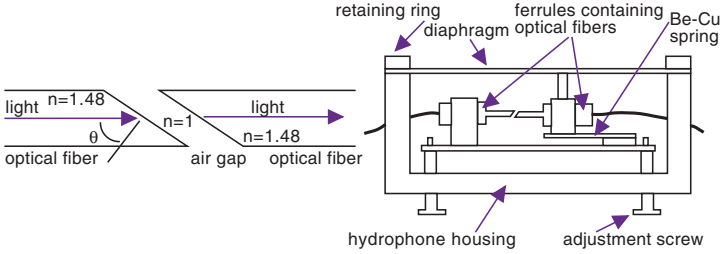

The theoretical sensitivity of optical transmission between the two fibers based on fiber gap has been calculated and compared with experimental measurements. The actual device was found to be more than an order less sensitive than the theoretical optimum.

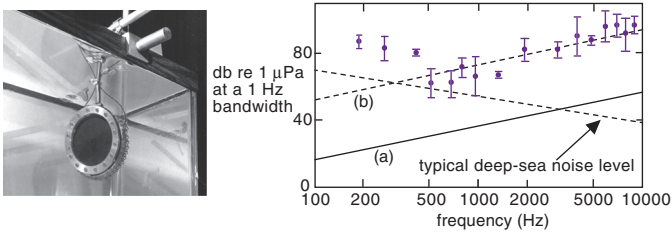

A hydrophone is depicted above in a test tank along with the results of its experimental evaluation. Curve (a) shows the minimum detectable pressure versus frequency assuming theoretical sensitivity to vertical fiber displacement, whereas curve (b) uses the measured values.

FTIR Fluid-Level Sensor

The FTIR phenomenon can be used as the basis of a **fluid-level sensor**. In this sensor, a multimode optical fiber is wound around disks adjacently arranged in a plane along a common vertical axis. This configuration is placed in a fluid tank with the vertical axis normal to the fluid surface so that as the tank is filled, the fiber around the largest diameter disk is covered first, and the fiber around the smallest diameter disk is covered last. The core and cladding modes are excited in the fiber but subjected to TIR when the fiber is exposed to air. Because the fiber is covered with fluid, FTIR occurs over the covered fiber length, and light is lost from the fiber. The decreasing diameter disks are intended to couple core modes into the cladding to replace light lost by FTIR.

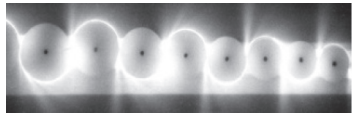

increasing fluid height
(vertical is to the right) →

The normalized detected optical power as a function of the fluid (water) height is shown below.

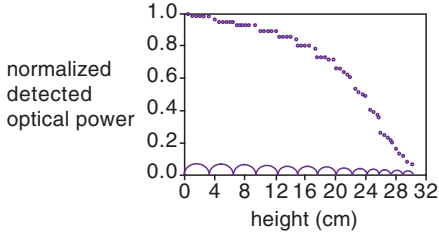

A fit to this data, where P is the normalized detected optical power and h (cm) is the fluid height, yields

$$P(h) = 1 - 3.5 \times 10^{-3}h + 1.5 \times 10^{-5}h^2 - 3.3 \times 10^{-5}h^3$$

Microbend Sensor Theory

Microbending can be used as a loss-modulating transducer mechanism. When an appropriate **periodic stress** is applied normal to the axis of a multimode fiber, light is coupled out of the fiber through the conversion of propagating modes into radiation modes that are lost. The amount of loss is a monotonically increasing function of the stress applied to the fiber.

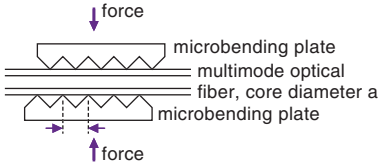

When a graded-index multimode optical fiber is used (the plastic buffer coating must be stripped away where the fiber is stressed), the optimum **deformer spacing** Λ is given by

$$\Lambda = \frac{2\pi a n_0}{NA}$$

where a is the fiber core diameter, n_0 is the index of refraction at the center of the core, and NA is the fiber numerical aperture. The following graph depicts the typical response for a Sumitomo graded-index fiber with $NA = 0.13$, $a = 23.27$ mm, and $n = 1.458$.

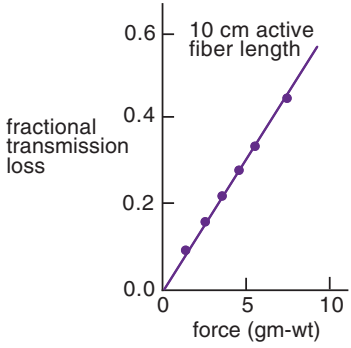

Microbend Pressure Sensor

A **microbend** transducer can be used as the basis of a high-temperature fiber optic **pressure sensor**. This design uses a twisted pair of optical fibers that are completely equivalent except that a segment of only one of the fibers is subjected to microbends within the sensor.

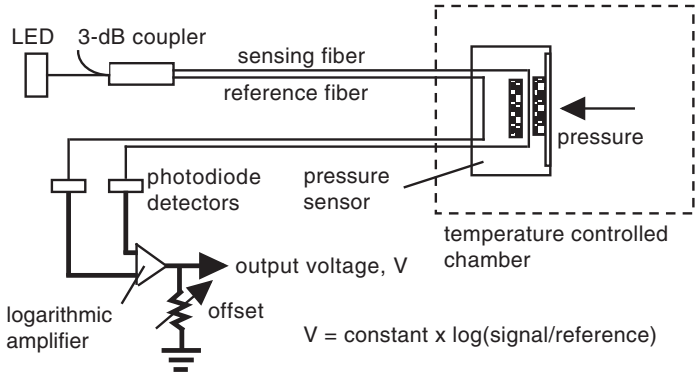

For this example, L is 2 mm, the LED center wavelength is 830 nm, the optical power propagating in the reference fiber is ~100 mW, and there are two periodic distortions of the fiber. The following graph shows the response of this sensor at two different temperatures.

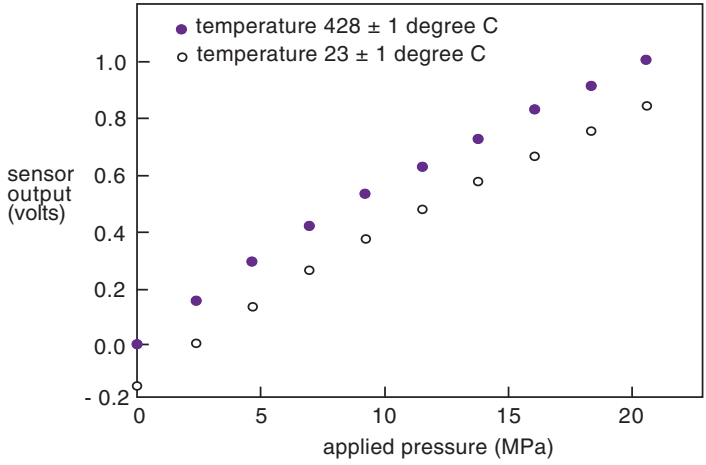

Macrobend Sensor Theory

Snell's law and the **Fresnel equations** govern the reflection/transmission of a light ray at a dielectric boundary. The plane defined by the light ray and the normal to the boundary at the point at which the ray strikes the boundary is called the **plane of incidence**. Angles are measured relative to this normal. If a light ray traveling in a medium of index of refraction n_1 strikes a boundary at an angle θ_1 with a medium that has a lower index of refraction n_2, then there will be some critical angle θ_c for which if $\theta_1 > \theta_c$, then all of the energy in the light ray will be reflected at an angle $\theta_3 = \theta_1$ back into medium 1. If $\theta_1 < \theta_c$, then some light will be transmitted into the second medium at an angle $\theta_2 = \sin^{-1}[(n_1/n_2)\sin\theta_1]$. The **reflection coefficients** for light polarized perpendicular to the plane of incidence (**s-polarized**) or lying within it (**p-polarized**) are R_s and R_p, respectively:

$$R_s = \left| \frac{n_1 \cos\theta_1 - n_2 \sqrt{1 - \left[\left(\frac{n_1}{n_2}\right)\sin\theta_1\right]^2}}{n_1 \cos\theta_1 + n_2 \sqrt{1 - \left[\left(\frac{n_1}{n_2}\right)\sin\theta_1\right]^2}} \right|^2;$$

$$R_p = \left| \frac{n_1 \sqrt{1 - \left[\left(\frac{n_1}{n_2}\right)\sin\theta_1\right]^2} - n_2 \cos\theta_1}{n_1 \sqrt{1 - \left[\left(\frac{n_1}{n_2}\right)\sin\theta_1\right]^2} + n_2 \cos\theta_1} \right|^2$$

The amount of light transmitted into medium 2 for an unpolarized light beam is then $T = 1 - [(R_s + R_p)/2]$. In terms of geometrical optics, the light propagating in an optical fiber is constrained to the core by TIR at the core–cladding interface. This constraint is removed when **macrobending** of the fiber occurs, effectively reducing the angle of incidence of the lowest-angle rays in the fiber until it is smaller than the critical angle for TIR, and some fraction of its power can be coupled through the core–cladding interface and radiated away. Macrobending can thus be used in loss-modulation transducers.

Macrobend Pressure Sensor

In a multimode optical fiber, **macrobending** changes the angles between certain propagating modes and the fiber cladding into angles that are less than the critical angle for TIR so that some optical power is radiated away into the cladding. The smaller the radius of curvature of the macrobend is, the greater the loss in transmitted optical power.

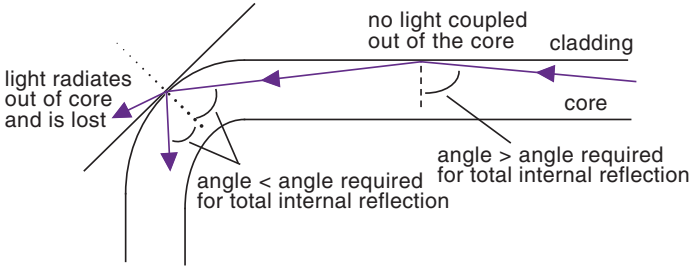

If a phenomenon of interest creates macrobending, a measurement of transmission loss can be used to infer its value. One of the first fiber optic sensors to use macrobending transduction was a **pressure sensor** that used a "**figure-eight**" configuration.

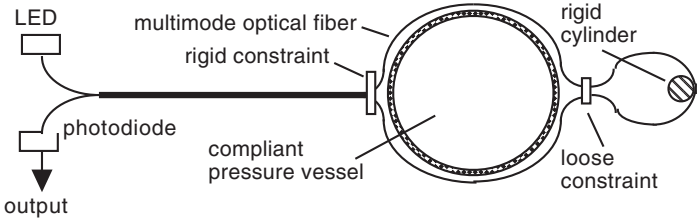

In this case, the change in diameter of a compliant pressure vessel changes the diameter of the larger part of the figure-eight loop, changing the diameter of the smaller loop and its macrobending loss. A simple variation of this technique is the "**slipknot**" macrobend strain transducer, in which the macrobends are unsupported.

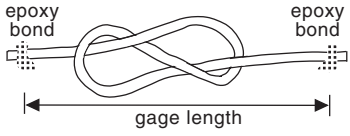

Modal Domain Sensor Theory

When a coherent source couples optical energy into a multimode optical fiber, that energy propagates along the fiber in the fiber's allowable modes. As these modes continue along the fiber, they interfere with each other so that if the light exiting the fiber were projected on a screen, a complex interference (or **speckle**) pattern would be observed.

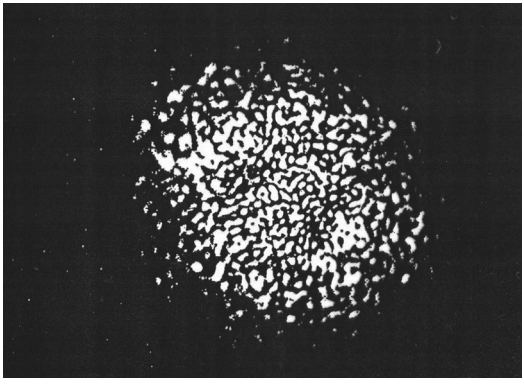

The speckles within the pattern are equivalent to a collection of the outputs of a number of interferometers whose phases, intensities, and modulation depths are operationally and randomly related within the constraint that the sum of all the intensities is a constant. Perturbation of the fiber along its length perturbs the individual elements of the speckle pattern—some intensities increase, some decrease, and some do not change—but their sum remains constant.

If the speckle pattern is projected on an array of optical diode detectors, then the sum of the outputs of those detectors will be independent of perturbation. However, the sum of the absolute values of the changes of those outputs will provide a very sensitive measure of the absolute value of the first time derivative of the integrated perturbation along the length of the fiber.

Modal Domain Vibration Sensor

A **modal domain** sensor configuration suitable for vibration measurements includes

- a laser diode coherent source,
- a multimode optical sensing fiber,
- a detector array with addressable individual elements, and
- suitable signal-processing electronics.

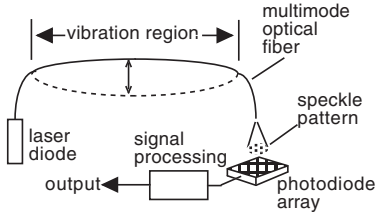

The most attractive feature of this configuration is the fact that digital signal processing can be used to create **virtual apertures** on the photodiode array, allowing various detection schemes to be evaluated. A small aperture produces a signal that follows the perturbation, but the signal is unstable and varies with environmental conditions. On the other hand, if the absolute values of the changes over Δt of each detector are summed, a very robust signal is produced that is proportional to the absolute value of the first time derivative of the vibration. Unfortunately, the nature of the absolute value operation destroys the phase information, making precise reconstruction of the perturbing signal problematic. There is an alternative approach that does not use a detector array, in which a **photochromic** filter mimics the detector array plus the absolute value summing process.

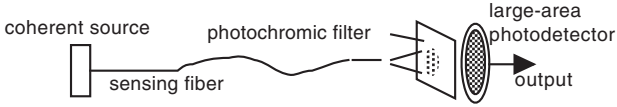

In-Line Fiber Coupling Theory

When the ends of two equivalent, polished multimode fibers are brought into proximity, the **coupling loss** between them can be used as a transducer mechanism. The two primary loss mechanisms used in simple fiber optic sensors depend on either axial or longitudinal displacement.

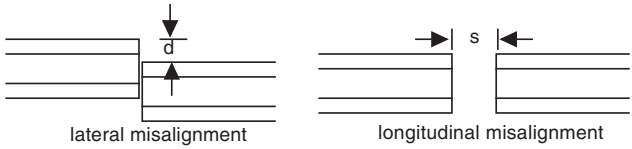

For a multimode step-index fiber with a radius a and **numerical aperture** $NA = 0.37$ [where the fiber critical angle $\theta_c = \sin^{-1}(NA)$], the fractional transmission T_A as a function of **axial displacement** is given by

$$T_A = \frac{2}{\pi}\cos^{-1}\left(\frac{d}{2a}\right) - \left(\frac{d}{\pi a}\right)\left[1 - \left(\frac{d}{2a}\right)^2\right]^{1/2}$$

whereas the fractional transmission T_L as a function of **longitudinal displacement** is given by

$$T_L = \left[\frac{1}{1 + \left(\frac{s}{a}\right)\tan\theta_c}\right]^2$$

These fractional losses are shown in the figure below:

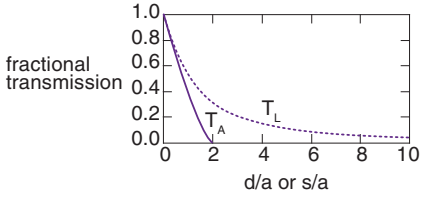

When both axial and longitudinal displacement are present, the situation becomes much more complicated.

Fiber Coupling Pressure Sensor

Fiber **coupling modulation** can be used as the basis of many fiber sensors; one interesting application is the **intracranial pressure sensor**. A schematic of the basic features of the sensor is shown below.

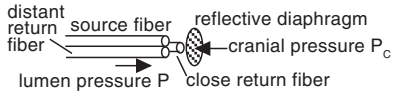

In this sensor, a thin flexible catheter has a reflective moveable diaphragm at its distal point. The catheter has a lumen that can be pressurized and that contains three optical fibers whose polished ends are in close proximity to the reflective diaphragm: one closer to the diaphragm than the other two that are located at the same distance. One side of the diaphragm sees the intracranial pressure P_c, whereas the other sees the adjustable pressure in the lumen. Light from the source fiber as shown reflects off the diaphragm and is coupled into both a fiber near the diaphragm and one further away. The optical powers detected by these two fibers vary with the distance of the diaphragm from the closest fiber.

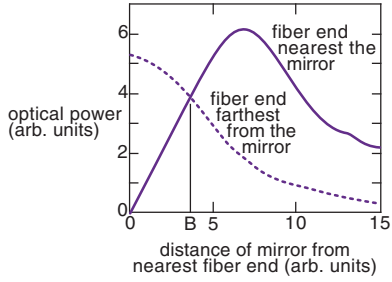

The mirror is pre-positioned so that when the lumen pressure equals the intracranial pressure B, the power coupled into the two receiving fibers is the same.

Polarization Theory

A monochromatic beam of light has an associated electric field that can be represented by a vector in the plane normal to the direction of propagation of the light. For red or near-infrared light, this vector oscillates at frequencies in the range of 2–5 $\times$ 10^{14} Hz. The **polarization** of the light is defined as a unit vector parallel to the same direction as the polarization vector of the light.

Because the frequency of light is much too large to allow the instantaneous polarization to be observed unless specialized techniques are used, the different types of possible polarization are qualitatively characterized by the trajectory mapped out by the tip of the polarization vector over one or more cycles of oscillation. The different general **possible polarizations** that a light beam can have are shown below, where the x–y plane is assumed to be normal to the direction of propagation of a light beam passing through the origin.

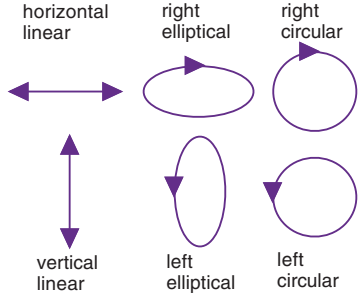

Some special sheet materials only allow transmission of that portion of a light beam whose polarization component is parallel to a linear direction in the sheet. These materials are called **linear polarizers**. If unpolarized light of intensity I_0 is incident upon one of the sheets and then passed through a second sheet whose transmission direction is at an angle θ to the first, then the intensity of the light exiting the second sheet will be

$$I = \frac{1}{2} I_0 \cos^2 \theta$$

Polarization Rotation Sensor

As an example of a simple intensity-modulating fiber optic sensor that uses polarizers, consider a requirement to monitor the **angular position** of a shaft whose angle can vary between 0 and 2π. One conceptual way of performing this measurement is shown below.

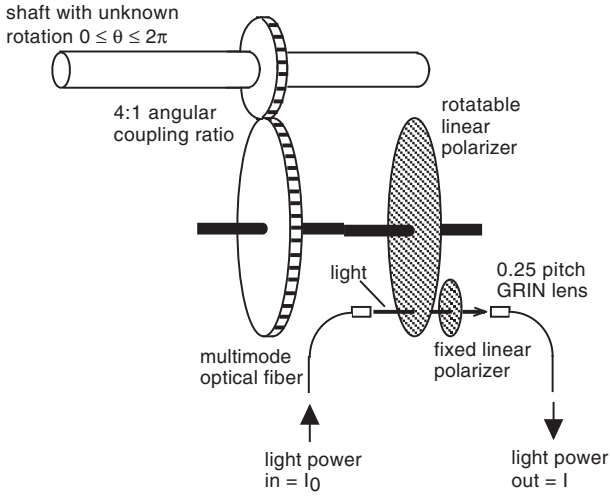

In this case, the shaft is fitted with a gear assembly such that one rotation of the shaft will result in one quarter of a revolution of a second shaft that has a coaxially mounted linear polarizer in front of a fixed linear polarizer. For 0 rotation of the shaft, the transmission axes of the polarizers are crossed, and no light can pass through them. For a rotation of 2π, the transmission axes are aligned, and a maximum amount of light power is transmitted. The initial optical power I_0 in a multimode optical fiber is collimated by a GRIN lens, passed through the two polarizers, and collected by a second GRIN lens that couples the output light I into a second multimode optical fiber. It is assumed that systematic optical transmission losses are accounted for in a fractional transmission factor α. Knowledge of I_0 and a measurement of I then determine θ:

$$I = \frac{1}{2} I_0 \alpha \left[1 - \cos\frac{\theta}{4}\right] \Leftrightarrow \theta = 4\cos^{-1}\left(1 - \frac{2I}{\alpha I_0}\right)$$

Photoelastic Sensor Theory

The **photoelastic effect** occurs when stress (or its induced strain) is applied to a suitable solid optical medium, such as glass, polycarbonate, or gelatin. If the stress is unidirectional, then the index of refraction (speed of light) for optical beams polarized parallel to the stress direction will directly depend on the stress. Light polarized in the direction perpendicular to the stress direction will not be affected.

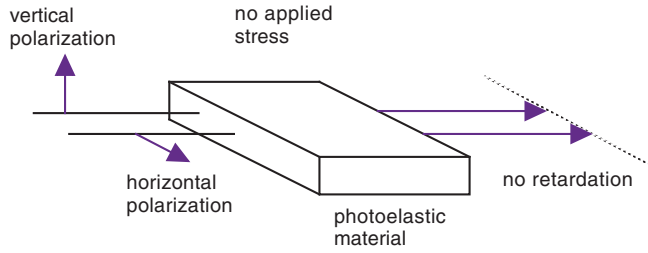

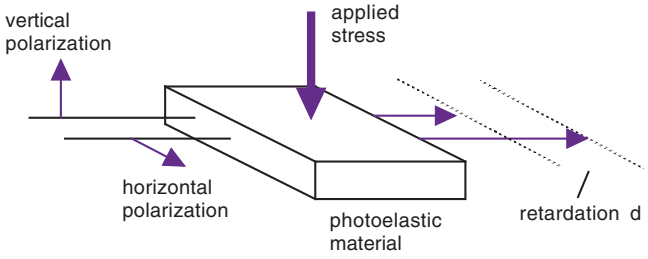

A photoelastic material under stress then acts as a stress-dependent **optical retarder** or waveplate that can serve as a transducer element in a fiber optic sensor. If light linearly polarized at an angle of $\pi/4$ to the stress direction is passed through a photoelastic material subjected to a linear stress s, then the output intensity I transmitted through a polarizer with its transmission axis along the $-\pi/4$ direction will depend on the stress and the stress-optic coefficient $f\sigma$ of the material.

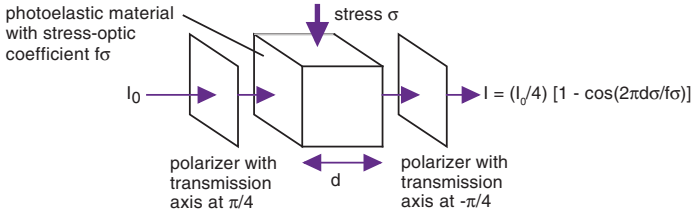

Photoelastic Pressure and Acoustic Sensing

Multimode photoelastic sensors have a number of applications, including **pressure sensing** and **acoustic detection**. These sensors use sophisticated optical arrangements and **difference/sum detection** for maximum performance.

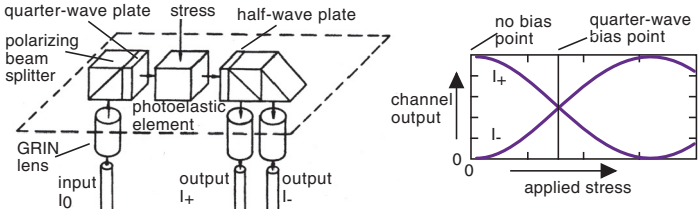

- In this case, the input light is collimated by a GRIN lens and then linearly polarized by a polarizing beamsplitter.
- A quarter-wave plate is used to convert the light from linear to circular polarization (effectively moving the output-channel bias point to its most sensitive location, as seen in the graph).
- The light then passes through the active photoelastic element and a half-wave plate to rotate the output polarizations by $\pi/4$ relative to the axes of a second polarizing beamsplitter for optimum response.
- The two output signals, I_+ and I_-, are then processed to produce a voltage proportional to $(I_+ - I_-) / (I_+ + I_-)$ such that variability due to environmental conditions is cancelled out.

The pressure sensor has a dynamic range of 120 dB with a minimum detectable pressure of 21 Pa. The acoustic sensor demonstrates a minimum detectable pressure of 47 dB re 1 mPa/Hz$^{1/2}$ at 500 Hz. The acoustic sensor and comparable electrical reference sensor are shown below.

Diffraction Grating Theory

If a light beam is projected on a screen and then an object blocks a portion of that beam with a sharp edge, the resulting shadow has a border region that is sharply defined but rather modulated. This physical effect is called **diffraction** and has been used as the basis for a number of fiber optic transducer mechanisms.

A diffraction grating, in its most basic form, is a plane of thin, transparent material whose surface has a large number of parallel reflective lines of width $d/2$ separated by transmissive regions also of width $d/2$. If a beam of light of wavelength λ is incident upon the grating in a plane defined by a normal to the grating and a second line normal to the lines within the plane of the grating, then the incident light at angle θ_0 will be diffracted at angle θ_D according to the **grating equation**:

$$d[\sin\theta_0 + \sin\theta_D] = m\lambda$$

where m is called the **diffraction order** and can be either a positive or negative integer ($m = 0$ implies no diffraction). The sign conventions associated with the grating equation are shown below.

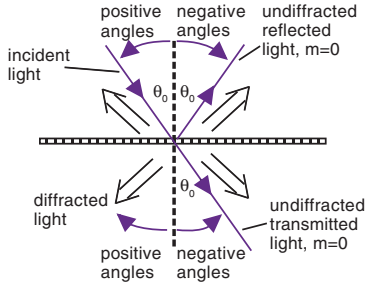

The sign of the order in reflection depends upon its position relative to the undiffracted reflected light:

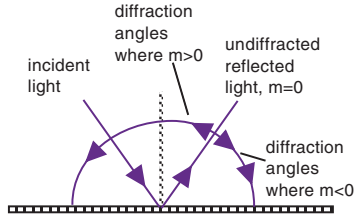

Diffraction Grating Rotation Sensor

A **diffraction grating** can be used as a transducer element to sense rotation. In this case, the diffraction angle equals the angle of incidence ($\theta_D = \theta_0$), so the **grating equation** becomes

$$2d \sin \theta_0 = \lambda$$

for 0 rotation of the shaft with an unknown rotation angle and $m = +1$ diffraction order.

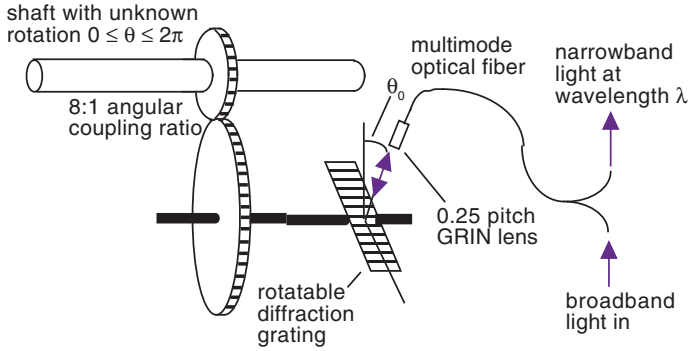

For non-zero unknown rotation θ of the shaft, the diffraction equation becomes

$$2d \sin\left(\theta_0 + \frac{\theta}{8}\right) = \lambda \quad \text{or} \quad \theta = 8\left[\sin^{-1}\left(\frac{\lambda}{2d}\right) - \theta_0\right]$$

If $\theta_0 = \pi/8$ is initially chosen for $\theta = 0$, so that for $\theta = 2\pi$ there is $\theta_0 + \theta/8 = 3\pi/8$, a choice of λ_1 (for $\theta = 0$) determines both the source spectral width $\lambda_1 \Leftrightarrow \lambda_2$ and the grating period d, or

$$d = \frac{\lambda_1}{2\sin\frac{\pi}{8}} \quad \text{and} \quad \lambda_2 = \lambda_1 \frac{\sin\frac{3\pi}{8}}{\sin\frac{\pi}{8}}$$

Because the quantities θ_0 and d are now known, a straightforward measurement of the wavelength λ uniquely determines the unknown **shaft-rotation** angle θ.

Although the sensor described here is not necessarily practical, the process is illustrative of the manner in which fiber optic sensors are designed.

Schlieren Grating Theory

Schlieren is a word borrowed from the German language to refer to streaks produced in a transparent medium. Diffraction gratings can be considered to have a Schlieren nature. In the field of fiber optic sensors, transducer mechanisms based on the relative motion of two aligned diffraction gratings have been called **Schlieren sensors**.

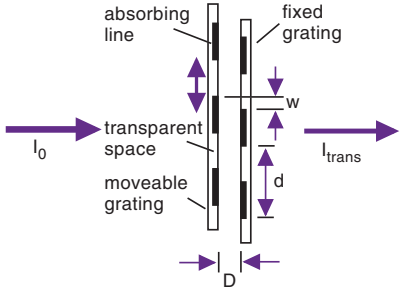

Collimated light from a multimode optical fiber is transmitted through the structure, and the zeroth diffraction order is captured by a second optical fiber. Modulation of the relative grating positions by a parameter of interest modulates the transmitted light (for a structure with $d = 10$ mm).

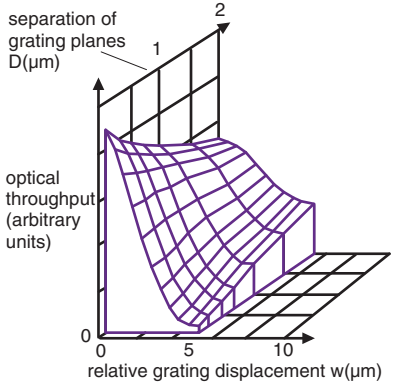

Schlieren Displacement and Acoustic Sensors

Multimode fiber optic sensors that use a Schlieren **opposed-grating structure** can be used to sense displacement and underwater sound. In this case, each of the opposed gratings has a period of 10 mm and transmissive stripes 5 μm wide.

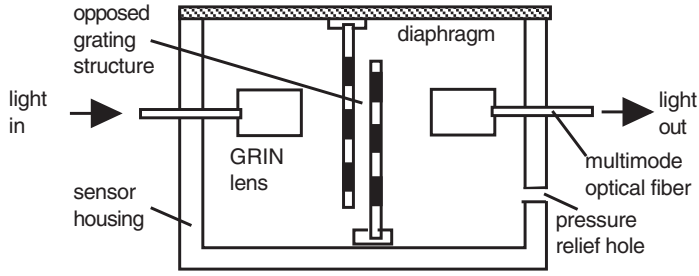

Light from a multimode optical fiber is collimated by a GRIN lens, coupled through the opposed-grating structure, and captured by a second GRIN lens and multimode optical fiber. This sensor is very sensitive to displacement and underwater sound.

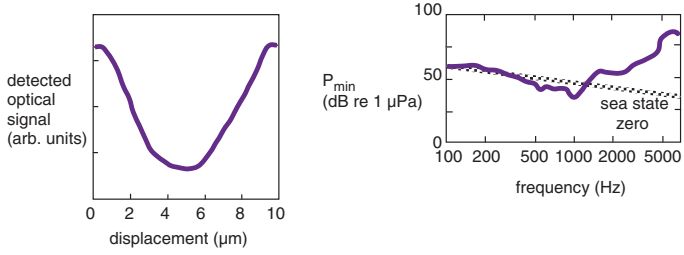

When a shot-noise-limited optical source is considered, this sensor has a displacement range approaching 5 μm and a minimum detectable displacement below 0.01 Å. When used to detect acoustic signals under water, the sensor is sensitive enough to detect acoustic pressure levels at sea-state zero (the acoustic noise level of a quiet ocean in the frequency range of 100–1000 Hz). The sensor is simple, cost effective, and does not require complicated signal-processing electronics.

Chirped Grating Sensor Theory

A diffraction grating is said to be chirped when its period d changes along its length, with the change usually being linear, i.e., $d = d_0 + d_1 x$, where x is the position along the grating, and d_0 and d_1 are constants. The most notable use for these gratings has been in wavelength-modulating **linear position sensors**. The most common method of creating such gratings involves the use of a photographic plate with a reflective backing, as shown below.

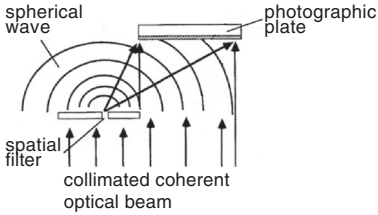

When such a **chirped grating** is used to detect displacement in the most basic configuration, the wavelength of a narrow-band, first-order diffracted signal determines the position x.

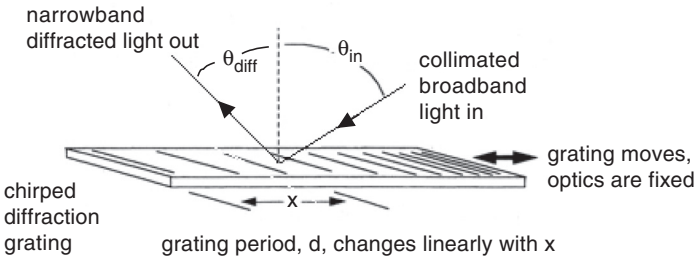

x depends linearly on the wavelength of the diffracted light (taking into account the angular sign conventions) according to

$$x = \frac{\lambda - d_0}{d_0(\sin\theta_{in} + \sin\theta_{diff})}$$

Chirped Grating Displacement Sensor

Chirped gratings can be used as the transducer mechanism for extrinsic fiber optic sensors for aerospace applications, especially in sensors that monitor the **aircraft actuator position**.

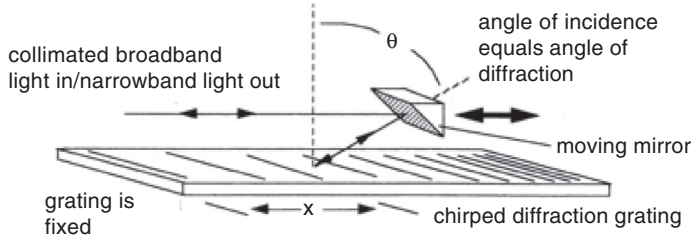

Because the angle of incidence and diffraction are the same, the detected wavelength determines the position of the grating according to

$$x = \frac{\lambda - d_0}{2d_1 \sin\theta_{in}}$$

where $d = d_0 + d_1 x$. The prototype sensor fits within a narrow cylindrical form factor to match a typical aerospace actuator.

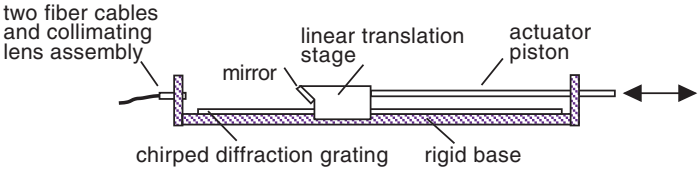

This particular sensor proves to be quite successful in meeting its performance goals:

- measurement range of 20 cm (7.9 in),
- linearity of ~1% in the raw output,
- resolution of 0.065 mm (0.0025 in), and
- bandwidth of 600 Hz.

Magneto-Optic Sensor Theory

A bulk **magneto-optic material**, such as glass, contains a collection of **magnetic moments** that are randomly oriented in the absence of an applied magnetic field so that there is no net magnetic moment. In the presence of such a field, these moments tend to align with the field, producing a net magnetic moment. Polarized light propagating through the material along the axis of its magnetic moment will have its polarization modified.

For thin magnetic films, the situation is quite different. Geometrical and energy constraints produce adjacent domains in which the magnetic moments are either up or down normal to the film plane. An applied magnetic field can modify the relative domain sizes or orientation of the moments within a domain but not their magnitude. Such a thin film, e.g., **bismuth-substituted iron garnet**, forms a polarization-independent optical phase grating whose properties can be modulated by appropriate applied magnetic fields. Monochromatic light incident upon such a grating will be diffracted along conical surfaces, and if the film has the proper thickness, then no light will be transmitted in the zeroth diffraction order for zero applied field.

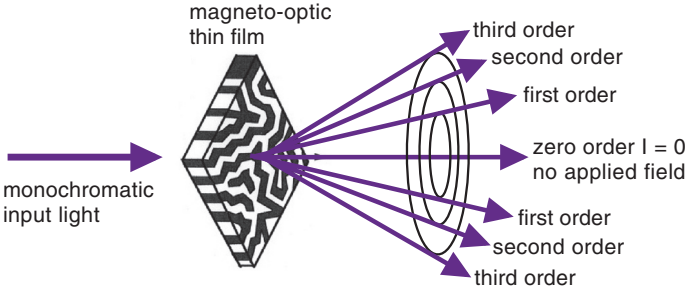

If a magnetic field is applied to the film normal to the film plane, domains with a moment aligned with the field will grow and those anti-aligned will shrink until the film is a single domain. The optical consequence of this is that the power in the zeroth order will grow from zero to some saturation value with an applied field.

Magneto-Optic Speed Sensor

Thin magneto-optic films can be used as the transducer mechanism for multimode fiber optic sensors, especially to sense **gas-turbine engine speed**. A schematic of the device is shown below along with a photograph of the assembled sensor with a dime coin for size comparison.

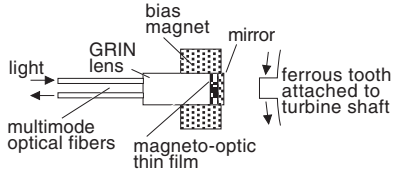

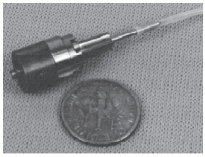

In this case, monochromatic light from a multimode optical fiber is collimated by a GRIN lens, passed through the magneto-optic film, reflected back through the film, and coupled via the same GRIN lens into an output fiber. A bias magnet provides a magnetic field that is modulated through the presence or absence of ferrous teeth on a rotating shaft. The sensor has been evaluated on a gas-turbine-engine test rig and found to be as good as or superior to conventional speed sensors used for the same application.

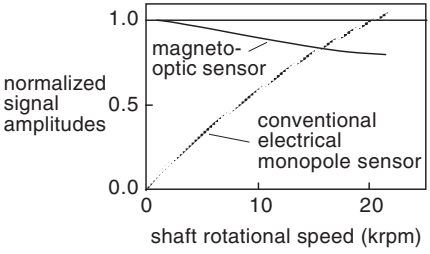

Optrode Sensor Theory

An **optrode** is the optical equivalent of an electrode. This simple device was first introduced for biochemical sensing in the United States through research supported by the **National Institutes of Health**.

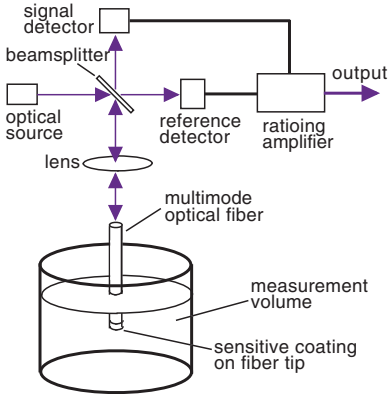

In this primitive version of an optrode, light from an optical source is split by a beamsplitter, with half of the optical power going to a reference detector and half collimated by a lens into an optical fiber. The optical fiber tip has a coating whose effective reflectivity depends on some parameter of interest in the measurement volume. The reflected light is then transmitted from the fiber through the lens and beamsplitter to a signal detector. The signal is divided by the reference in a ratioing amplifier, and the value of the ratio is output to a display. Based on the value of the ratio and the known characteristics of the fiber tip coating, the value of the parameter of interest can be determined.

Modern optrodes

- use an optical coupler instead of a beamsplitter,
- eliminate the lens, and
- can sense numerous parameters.

Optrode pH Sensor

Fiber optic optrodes can be used in a number of configurations with several different transducer mechanisms. One early optrode is very successful at measuring the **pH** of fluids; it incorporates a clear cellulose triacetate fiber with a sensing region made porous and sensitized by a **Congo Red pH indicator**.

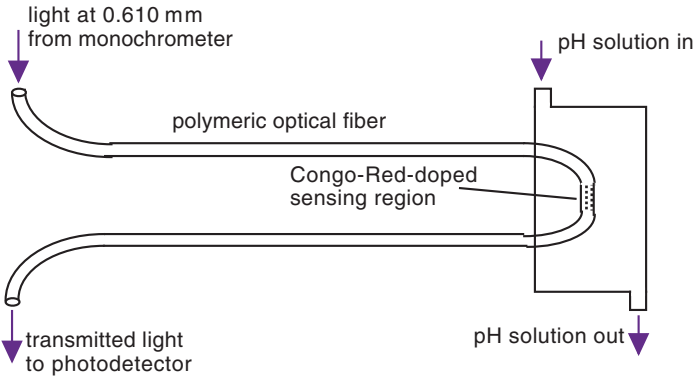

Light at 0.610 μm, matching the maximum sensitivity wavelength of response of the Congo Red, is coupled into the fiber, and the transmitted intensity is measured for solutions with a range of pH values. The absorbance of the optrode is found to vary monotonically with pH.

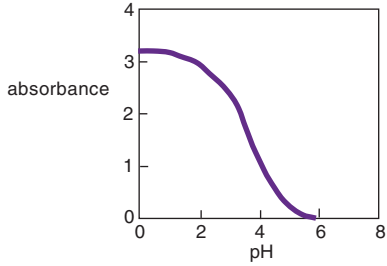

This extremely simple **through-transmission optrode** is inexpensive and sensitive, in addition to having a response that is reversible and repeatable. The device is insensitive to NaCl concentration in the fluid.

Fluorescence Theory

Fluorescence is a phenomenon that occurs when high-energy (short-wavelength) light is absorbed by certain materials, resulting in the temporary creation of a population of electrons in a highly excited state. When the exciting signal is turned off, the **excited electrons** begin to decay to intermediate empty states, emitting photons in the process. These photons are of lower energy and have longer wavelengths than the exciting signal.

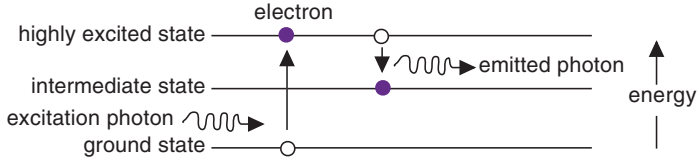

The lower-energy photons are called the fluorescence of the material. For the purpose of being used as a transducer in fiber optic sensors, the phenomenon of fluorescence has two attributes of interest:

- When the excitation signal is turned off, the power of the fluorescence decays with time.
- The fluorescence process can be **quenched** and its optical signal reduced or eliminated when certain chemical species interact with the fluorescent material.

For an initial population of N highly excited electrons with a fluorescent decay probability of $\alpha(s^{-1})$, an integrated fluorescent optical signal $S_n = \alpha N\,(1 - \alpha)^n$ will be produced during the interval between the n^{th} and $(n + 1)^{\text{th}}$ second after the population of N highly excited electrons is created. This signal decay is illustrated below.

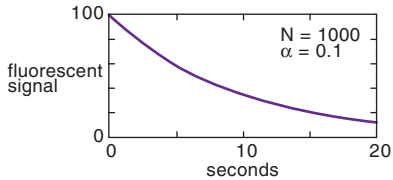

The temperature dependence of the signal-decay constant can be utilized to determine temperature.

Fluorescence Temperature Sensor

Fiber optic sensors can use the phenomenon of **fluorescence** as the basis of a transducer mechanism. The earliest demonstrations of the potential of fluorescence transduction for sensing temperature assumed that the fluorescent e^{-1} **decay time** τ is related to the absolute temperature according to

$$\tau = \frac{1 + e^{(-\Delta E/k_B T)}}{R_E + R_T e^{(-\Delta E/k_B T)}}$$

where k_B is Boltzman's constant; ΔE, R_E, and R_T are constants; and T is the absolute temperature in kelvins. The optical fiber probe utilizes a single strand of 600-μm plastic-clad silica fiber that is bonded to a lutetium–aluminum–chrome–borate $[Lu(Cr_xAl_{1-x})_3(BO_3)_4]$ crystal with a chrome content of 0.01. This particular crystal has the temperature dependence of τ shown below.

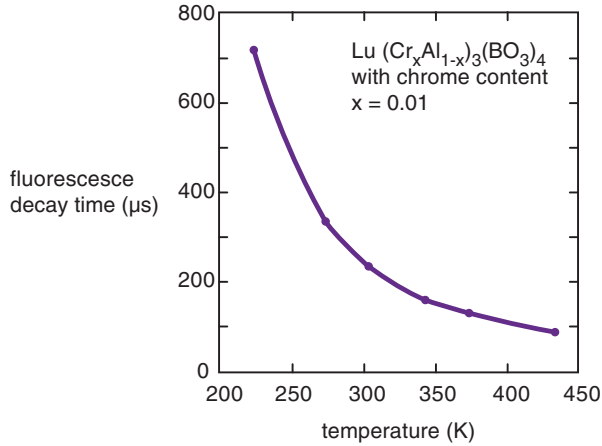

This sensor allows for the accurate determination of temperature from 273 K (0 C) to 340 K (70 C), with a standard deviation of consecutive measurements of 0.04 K.

Blackbody Theory

The concept of the **blackbody** was first introduced in the middle of the 19th century by G. Kirchhoff, who stated,

> "... bodies can be imagined which, for infinitely small thicknesses, completely absorb all incident rays, and neither reflect nor transmit any. I shall call such bodies *perfectly black*, or, more briefly, *black bodies*."

The current definition of a blackbody is one that captures all incident radiation at all angles and absorbs it all. A small opening into a cavity made of absorbing material serves as a good approximation of a blackbody.

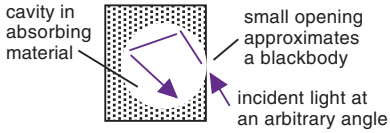

If a blackbody is in thermal equilibrium, it emits electromagnetic radiation according to **Planck's radiation law**, i.e.,

$$F(\lambda) = \frac{2\pi hc^2}{\lambda^5 (e^{hc/k_B \lambda T} - 1)}$$

where F is the emitted power at wavelength λ, h is Planck's constant, c is the speed of light, k_B is Boltzman's constant, and T is the absolute temperature. The spectra changes with equilibrium temperature, as shown below.

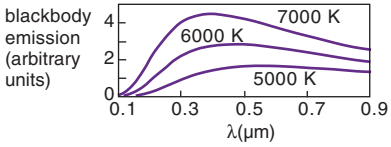

As can be seen from this figure, the total power emitted increases with the absolute temperature, whereas the peak of the spectrum moves toward shorter wavelengths according to **Wein's law**:

$$\lambda_p = 2900/T$$

Blackbody Temperature Sensor

Fiber optic temperature sensors based upon blackbody emission were among the first fiber optic sensors to be developed and commercialized.

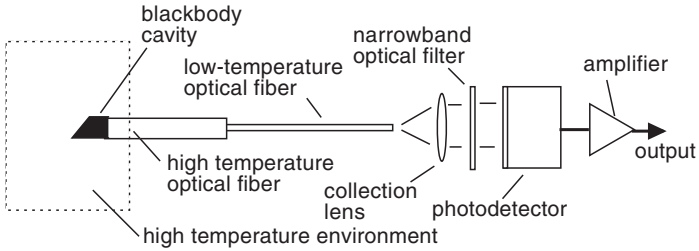

The basic sensing configuration consists of

- a **high-temperature optical fiber** on which an effective **blackbody cavity** has been fabricated,
- a low-temperature optical fiber, and
- signal conditioning, including a collection lens, narrow-band optical filter, photodetector, and amplifier.

A high-temperature optical fiber (sapphire) is required for this application because glass optical fibers would melt at the extreme temperatures of device operation. The blackbody cavity was created by sputtering a platinum coating on the beveled end of the high-temperature fiber. The low-temperature fiber is a standard multimode silica fiber with a core diameter of 600 μm, and the narrow-band filter has a center bandpass wavelength of 0.6 mm. After calibrating the sensor at a single temperature (with an output proportional to the optical signal), arbitrary temperatures can be determined using Planck's radiation law. This sensor is extremely accurate.

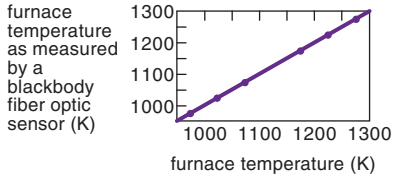

Optical Time Domain Reflectometry Theory

Optical time domain reflectometry (OTDR) is a technique that is commonly used to interrogate fiber optic cables to detect and localize regions of excess loss.

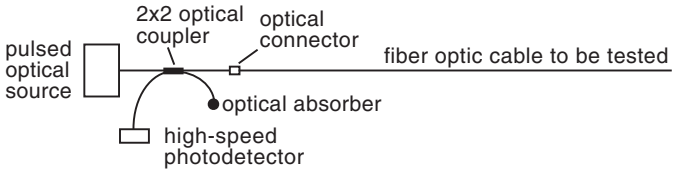

In this instance, a very short high intensity optical pulse is injected into the optical coupler and then passes into the fiber optic cable to be tested. Due to small imperfections, as well as variations in the index of refraction, a small amount of backscattered light is created as the initial pulse passes through each region of the fiber in the cable. This **backscatter signal** travels back up the cable to the optical coupler, where it is quantified as a function of time after the initial pulse injection by high-speed-detection and signal-conditioning electronics. The following figure depicts a typical backscatter signal versus time (proportional to the distance along the fiber).

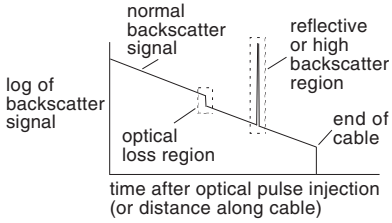

A region of optical loss in the fiber results in an offset of the normal backscatter signal. The magnitude of this offset allows the optical loss to be determined. If a region of high reflection/backscatter exists, a peak in the signal will occur. If the fiber length is continually eroded by some phenomenon of interest, the spatial progress of that phenomenon versus time can be determined using OTDR end-of-fiber "point" measurements versus absolute time.

Optical Time Domain Wavefront Speed Detector

One of the key parameters in characterizing the effects of explosive devices, whether nuclear or conventional, is the so-called **velocity of detonation** (VOD), which is the speed at which the destructive **blast wave** from the explosion propagates through the medium in which the explosion occurred. In principle, **OTDR** would be an ideal method of making this measurement (whereby an optical fiber is laid from the planned site of the explosion to a distant location) and then monitoring the length of the fiber as a function of time (the blast wave sequentially destroys the fiber and reduces its length). Unfortunately, standard OTDR processing is too slow for this application, but there is an OTDR alternative.

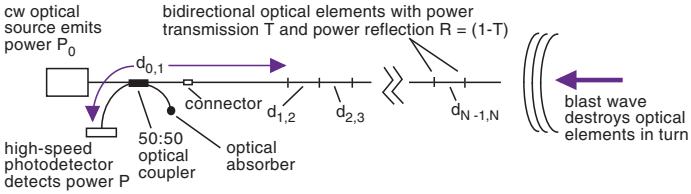

As each optical element (assuming $N = 10$) is destroyed, the detected optical power is reduced in a stepwise fashion.

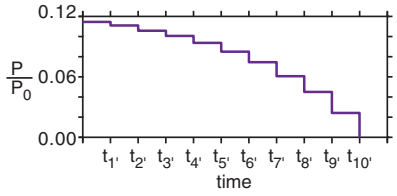

The actual time of destruction of the i^{th} element is given by $t_i = t_i' - D_i/c$, where c is the speed of light in the fiber, and D_i is the distance along the fiber from the photodetector to the i^{th} element. Because the time of destruction of each element is known along with its position, the VOD can be determined along the fiber path.

Evanescent-Wave Theory

An optical fiber guides light with minimal loss along a core region of material. The electric field associated with each fiber optical mode also extends into the material surrounding the core, whether this is the fiber cladding, buffer coating, environmental material, or some combination thereof. The electric field that exists outside the core is called the **evanescent field**, and its magnitude decays exponentially with the radial distance from the core interface.

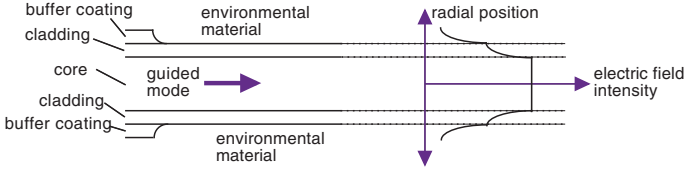

The evanescent field can be made to interact with claddings whose properties are sensitive to chemical or biological agents or with the environmental material directly. In both cases, the fiber buffer coating must be removed. The electric-field interaction with the phenomenon to be measured will then manifest itself in some form of modulation of the overall fiber transmission characteristics, and this modulation can be used to quantify the phenomenon of interest. To optimize evanescent-field transduction, the maximum amount of mode energy must be made to propagate outside the core region so that the most mode energy can interact with the phenomenon of interest. This can be done by

- exciting the fiber with only very-high-order modes near the cut-off angle for TIR,
- tapering the fiber into the transduction region,
- partially or totally removing the cladding in the transduction region, or
- using a very small core fiber, among other techniques.

A **tapered-fiber** evanescent-wave transducer increases the amount of evanescent wave and captures it again after its interaction with the phenomenon of interest.

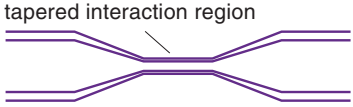

Evanescent-Wave Chemical Sensor

An example of a fiber optic **evanescent-wave chemical sensor** uses a tapered multimode optical fiber to detect small concentrations of **methylene blue dye**.

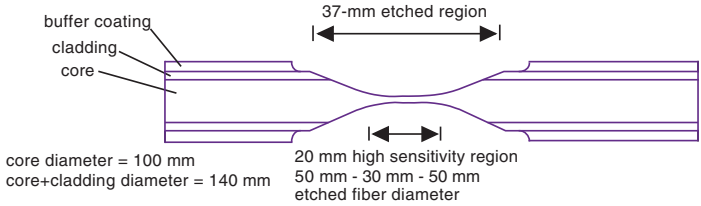

The fiber is etched over a 37-mm length with outer fiber diameters from 140 μm at the start to 50 μm at 8.5 mm, 30 μm at 18.5 mm, 50 μm at 28.5 mm, and back at 140 μm at 37 mm. Light from a He-Ne laser at 0.6328 mm is passed through an optical fiber coupler, one arm of which is used to provide a reference signal, and another consists of the sensing fiber. Without any concentration of dye, ~1.3% of the injected optical power is available to interact with water around the fiber core. Measurements of transmitted power are made for pure water and water with concentrations of dye equal to 1, 5, and 10 parts per million (ppm). These measurements are also converted to optical density $OD = -\log_{10}(I/I_0)$, where I_0 is the transmitted power for pure water, and I is transmitted intensity. Concentrations as low as 1 ppm can be detected.

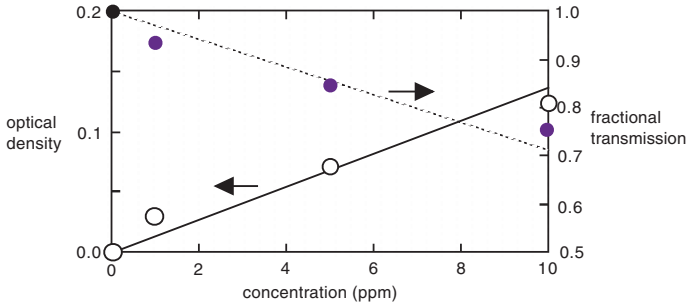

Single-Mode Interferometers

The initial interest in fiber optic sensor technology for high-performance devices was heavily focused on the interferometeric fiber sensor, primarily the **Sagnac interferometer** that is the basis for fiber optic rotation sensors and the **Mach–Zehnder interferometer** used to support acoustic sensing. The development of key components allowed the usage of the Michelson interferometer in application areas that were previously dominated by the Mach–Zehnder interferometer. In all cases, interferometeric fiber optic sensors depend on mixing two or more light beams.

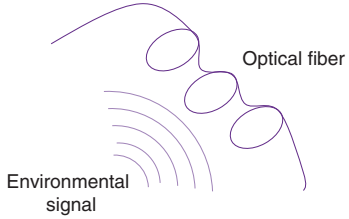

Phase differences are extracted with high precision and sensitivities that are often measured in sub-microradians. The path differences are generated by a delay between the arrival of two light beams, and the resulting relative phase shift $\Delta\phi$ is given by

$$\phi = 2\pi nL/\lambda = nL\kappa$$

where n is the index of refraction, L is the physical length of the fiber, λ is the wavelength of light, and $k = 2\pi/\lambda$ is the wavenumber. For small variations, the phase delay can be found by differentiation:

$$d\phi/\phi = dL/L + dn/n + dk/k$$

In the case where the wavelength is held constant, the two remaining terms depend on the variation in fiber parameter, i.e., the length L of the optical fiber changes and the index of refraction changes of the optical fiber. Wavelength variations can be used effectively to extract small phase differences.

Mach–Zehnder Interferometers

The **Mach–Zehnder interferometer** consists of a light source that, for optimal performance, is usually a frequency-stable, single-wavelength source that couples light into a beamsplitter. This device generates two light beams that pass through a reference leg and a signal leg. The primary purpose is to cause an environmental effect to generate a net phase difference between the two legs of the interferometer. The light beams are mixed and fall onto one or more output detectors.

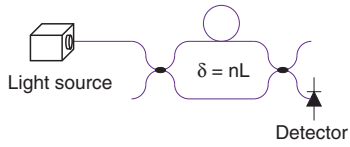

One immediate issue is that if the two optical beams traverse exactly the same optical path in the Mach–Zehnder, it will minimize sensitivity to small signals. Early implementations resolved this difficulty by placing a piezo-electric stretcher in one leg of the interferometer and continually readjusting it for the highest sensitivity. This can be done automatically by inducing a small variation in the path length—a **dither**—and maintaining its amplitude. A more practical approach is to intentionally have the two legs of the interferometer have different lengths L_1 and L_2. By varying the frequency of the light source sinusoidally, a phase dither can be established:

$$\phi_{\text{dither}} = \Delta F \sin(\omega t)(L_1 + L_2)n/c$$

The first harmonic on this output on the detector is proportional to the sine of the phase, and the second harmonic is proportional to the cosine. Differentiating and cross-multiplying allows the phase to be extracted directly. This is called **quadrature detection**.

Mach–Zehnder Hydrophone

The Mach–Zehnder interferometer can be configured to sense a variety of environmental effects. The first major application involved fiber optic hydrophones for naval applications. The typical configuration consists of a hollow mandrill wound with an overlapping optical fiber. In the simplest configuration, one end of the sensing fiber is attached with an adhesive, the rest of the fiber leg is wound under tension, and the second end is secured.

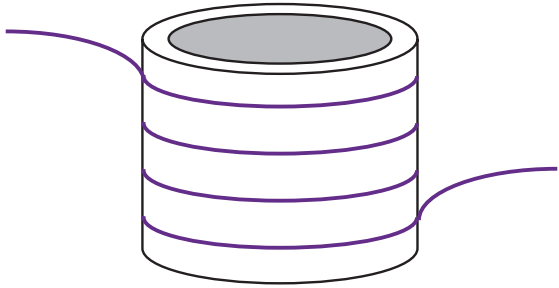

To avoid thermal effects, the reference leg of the hydrophone is wrapped parallel to the sensing fiber leg. Several approaches have been used to attain a differential response. A commonly employed method uses an optical fiber with a coating that enhances the acoustic response, such as a nylon-coated fiber, next to one with a reduced response, such as a polyimide-coated fiber. The hollow mandrill is intended to act as a mechanical amplifier, expanding and contracting with acoustic waves, which varies the tension on the optical fibers.

Directional sensitivity can be obtained by optimizing geometries and by winding the optical fiber into a ball; the sensor can be omnidirectional.

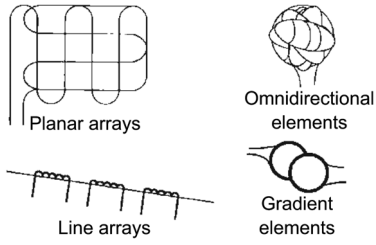

Mach–Zehnder Transducer Geometries

The Mach–Zehnder (and Michelson) interferometer can be used to sense seismic events by using a push–pull arrangement, where the upper and lower rubber mandrills are wound with the two fiber sensing legs of the interferometer. When a mass is placed between these weights and the casing is attached to the ground via a spike, ground motion causes one mandrill diameter to expand and the other to decrease, resulting in a differential difference in the optical path length between the two legs.

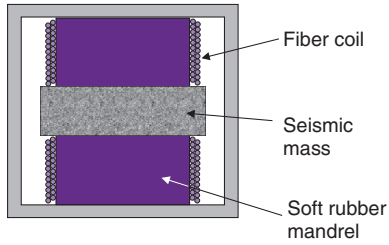

Another common transducer involves mounting an optical fiber on a strip of material that is sensitive to an environmental effect. For magnetic fields, this could be a strip of Metglas® or a magneto-strictive material, such as nickel. The fiber can be simply bonded to the surface.

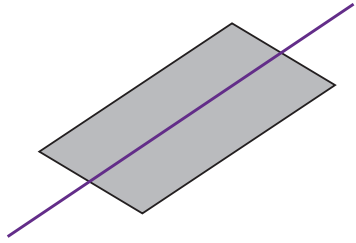

Another common approach that can be used to configure a transducer involves using special coating materials that will enhance a specific environmental effect and/or using these materials for an underlying mandrill. Typical materials include

- nylon or Hytrel® for acoustics,
- nickel or Metglas® for magnetic fields, and
- PVF for electric-field applications.

Michelson Interferometer

The layout of the **Michelson interferometer**, like the Mach–Zehnder interferometer, has two sensing legs, and the objective is to optimize the differential phase response of the two legs to a specific environmental effect. The major difference is that it is configured with mirrors on the end of each sensing leg and is operated in reflection. Because the single-frequency light sources that were initially available were extremely sensitive to reflections, the Mach–Zehnder version, which avoided back reflection, was the first to be heavily developed.

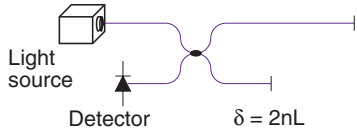

A series of technical innovations of components have completely changed the situation for modern acoustic and seismic applications. The first is the availability of super-stable single-frequency light sources that, in combination with optical isolators developed for the telecommunication industry, have greatly reduced noise due to feedback from reflected light. The second major development is the usage of **Faraday mirrors**.

One of the principal problems associated with dual-leg interferometers is that the light sources they use are highly polarized, and the polarization can evolve differently along each sensing leg. It is possible that when the two beams recombine the light beams have orthogonal polarization states, resulting in complete signal fade out. The Faraday mirrors convert the reflected light polarization state so that it moves back through the same set of polarization states and the two beams will combine at the beamsplitter at the original polarization state.

Sagnac Theory

In the early 1900s, a demonstration was conducted by **Georges Sagnac** that if light could be made to propagate clockwise and counterclockwise about a closed path, and if the path were rotated quickly enough, changes in a fringe pattern associated with the combined beams could be observed.

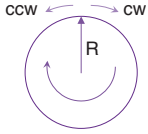

cw path: $2\pi R + RL/c$

ccw path: $2\pi R - RL/c$

Net path difference: $2\,RL/c$

$Z_R = 2\,RL/(\lambda c)$

When the loop is rotated clockwise, the light beam moving in this direction must go a little further than the counterclockwise beam, which must go a shorter distance by an equal and opposite amount. When the two beams are combined, the resulting fringe shift is simply the difference in path length divided by the wavelength of light propagating around the closed path. Monitoring this fringe position is the underlying principle behind the open-loop fiber optic gyro.

For higher performance, a **closed-loop approach** can be achieved by introducing a frequency shift between the counterpropagating light beams.

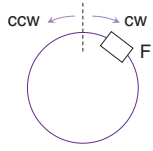

$Z_{Fcw} = (F_o + F)(Ln/c)$

$Z_{Fccw} = F_o Ln/c$

$Z_F = FLn/c$

Setting $Z_R = ZF$
Renders $F = 2R/\lambda n$

Rotationally induced fringe shifts can be counterbalanced by fringe shifts induced by frequency differences between the two light beams over portions of the closed path offset from the center of the path. Forcing the two fringe shifts to offset results in a frequency proportional to rotation rate Ω.

Sagnac Rotation Sensor/Fiber Optic Gyro

The **Sagnac rotation sensor/fiber optic gyro** can be implemented in open- or closed-loop formats.

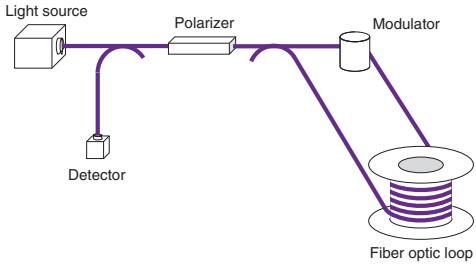

Open-loop fiber optic gyro

The open-loop format utilizes a low-coherence light source, a polarizer, and two beamsplitters to establish a reciprocal light path between the clockwise- and counterclockwise-propagating light beams. A modulator is used to establish a signal out of the noise, and polarization control may be in the form of a polarization-maintaining optical fiber.

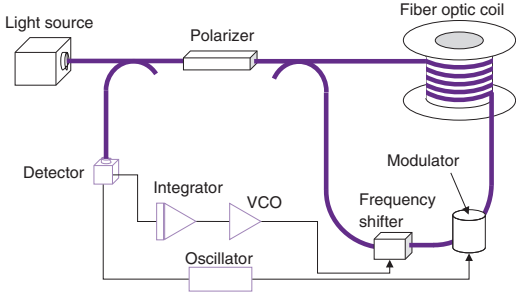

Closed-loop fiber optic gyro

In this version, the modulator varies the optical path length between counterpropagating light beams. If this is done sinusoidally, the even and odd harmonics appear on the detector as the two beams combine and interfere. If the two beams are perfectly in phase, then only even harmonics appear. The odd and (in particular) the first harmonic signal can be used in the open-loop gyro to indicate the magnitude and direction of rotation. In the closed-loop setup, the first harmonic can be used as an error signal to readjust the frequency needed to close the loop.

Sagnac Acoustic Sensor

The Sagnac interferometer can be utilized as an acoustic sensor. When an acoustic signal that is a time-varying pressure wave arrives at a portion of the fiber loop associated with the Sagnac interferometer that is offset from the center position of the loop, an optical path length difference between the two counterpropagating light beams is induced.

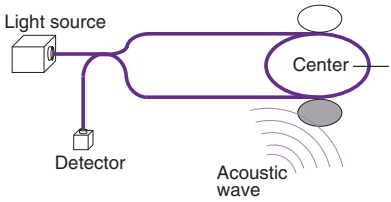

The magnitude of the path length difference depends on the spatial position of the acoustic beam and its frequency. For a sinusoidal signal at frequency ω, where half of the fiber loop length is shielded and the other half has a response per unit length A and a magnitude of the acoustic signal B, the response of the **Sagnac acoustic sensor** has the form

$$R[P(t)] = [ABnL^2/4c]\,\omega\sin(\omega t)$$

The response depends on the square of length L of the loop and is directly proportional to the frequency of the signal for frequencies that are small compared to the fundamental frequency of the Sagnac loop (the inverse transit time of light through the loop).

Principle advantages of the Sagnac interferometer:

1. a low-coherence light source that can inherently be very low noise and cost effective,
2. an adjustable response that rapidly increases with fiber length, and
3. optical filtering of low frequency noise.

Optical power I can also be used to identify the location of a time-varying signal that can be used to detect leaks in pressurized structures and the location of intruders.

Sagnac Interferometer Strain Sensor

The Sagnac interferometer can be used as a long-gage-length strain sensor with lengths up to tens of kilometers. The layout consists of a broadband light source that is used with a central beamsplitter to generate counterpropagating light beams in the Sagnac loop. A frequency shifter is introduced near one side of the loop, which introduces a frequency difference F between the two light beams.

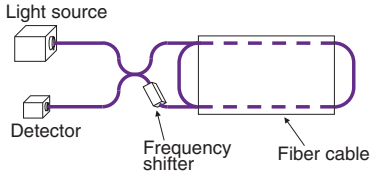

The frequency-induced fringe shift between the two counterpropagating light beams is given by $Z_F = F(Ln/c)$. Suppose that the **Sagnac strain sensor** is operated so that the frequency is adjusted by locking onto one fringe peak. The condition is then $Z_F =$ constant.

Differentiating the fundamental equation results in

$$0 = dF(Ln/c) + FdL(n/c)$$

and the final result $dF/F = -dL/L$.

As a specific example, suppose that the frequency shifter introduces a difference of 100 MHz between the counter-propagating light beams, and the system can resolve frequency changes of 1 Hz. This would mean a resolution of the system of one part in 10^8 and, for a 1-km-long fiber loop, the ability to resolve length changes of 10 microns. The fiber loop could be integrated into a cable and used as a very long strain gage. Care must be taken to minimize thermal and acoustic effects by appropriate geometric placement of the optical fibers.

Bragg Grating Fabrication

Bragg gratings can be formed in a single-mode optical fiber through two major methods. The first takes a laser beam and folds it into two paths that intersect on the optical fiber, forming bright and dark regions. For short-wavelength light beams and Ge-doped optical fibers, the local index of refraction is changed along the length of the core via changes in the Ge-Si dioxide bonds. If the laser beam is sufficiently intense and short, an index-of-refraction change can be induced by localized damage. These short pulse gratings can be stable up to the melting point of the optical fiber. For lower-intensity light beams, the specifics of the process will limit temperature ranges. Post-process annealing is usually performed at 50 °C above the maximum operating point to ensure long-term thermal stability. The wavelength of the Bragg grating can be controlled by the angle between the two intersecting optical light beams.

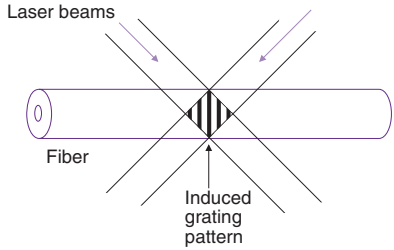

Another approach uses a single laser beam and a phase mask to form an interference pattern that can be used to form Bragg gratings on an optical fiber. This setup is less costly to implement, but changing wavelengths involves purchasing additional phase masks, which can be expensive.

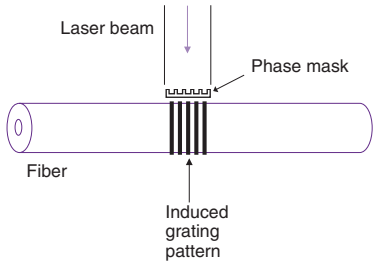

Bragg Grating Theory

Implementation of **Bragg grating** sensors, in its simplest form, involves changing the physical separation between the periods of the grating via an environmental effect. The most common examples are axial strain and temperature. In the case of temperature the change in wavelength due to a temperature change is given by

$$\delta\lambda/\lambda = (\alpha + \zeta)\Delta T$$

where α is an expansion coefficient that equals 0.55×10^{-6} $^{\circ}C^{-1}$ for silica, and ζ is a thermo-optic coefficient for the fiber core material, which equals 8.31×10^{-6} $^{\circ}C^{-1}$ (estimated for GeO_2 doping):

$$\delta\lambda/\lambda = 8.86 \times 10^{-6}\Delta T$$

For axial strain, the response of the wavelength to strain changes is

$$\delta\lambda/\lambda = (1 - p_e)\varepsilon$$

where p_e is the photoelastic constant, which equals $(n^2 / 2)$ $[p_{12} - \nu(p_{11} + p_{12})] = 0.22$ for silica:

$$\delta\lambda/\lambda = 0.78\varepsilon$$

There are slight variations in these parameters depending on the exact geometry of the optical fiber and the dopant material used to generate the core and cladding. For the 1300-nm wavelength of light, a change in wavelength of 10 pm corresponds to a change in temperature of 1 °C. In the case of strain at 1300 nm, a 1-pm wavelength change corresponds to 1 microstrain. At 1555 nm, the other very common telecom wavelength, 12 pm corresponds to 1 °C and 1.2 pm to 1 microstrain.

These cases involve bare fiber. When the fiber grating is attached to a substrate, that material will modify the response.

Bragg Grating Simultaneous Strain and Temperature

The simplest implementations of fiber Bragg gratings involve measuring the longitudinal strain and temperature. In the case of longitudinal strain, the fiber grating can be either

- attached continually to a surface using strain gage cement or
- pre-strained and anchored at two points across the grating.

In the case of temperature, the fiber grating should be unstrained; the most common approach places it in a loose tube anchored at one end.

There are two approaches to measure both axial strain and temperature simultaneously at the same location.

- One uses dual overlaid fiber gratings at different wavelengths. If the wavelengths are sufficiently separated, then there are two equations in two unknowns that can be solved. The principal issue with this approach is that the wavelengths must be separated by a large enough difference to have a well-conditioned set of equations that can be solved with sufficient accuracy, and two light sources are required for a conventional fiber.
- A second approach writes a single fiber grating onto a birefringent optical fiber, which can be a commercial polarization-preserving optical fiber. Each of the birefringent axes produces a wavelength, and two equations in two unknowns result. The condition of the matrix depends on the wavelength and properties of the birefringent fiber.

Bragg Grating Transverse Strain

The Bragg grating may also be configured to measure **transverse strain**. In this case, the fiber grating is again written onto a birefringent optical fiber, such as a commercially available polarization-preserving fiber. A single grating of this type, when illuminated by a broadband light source, has dual peaks. The polarization-preserving fiber is constructed with materials that have different hardness, which results in a difference in stress along the two transverse axes p and q.

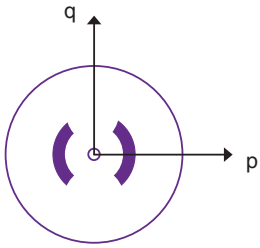

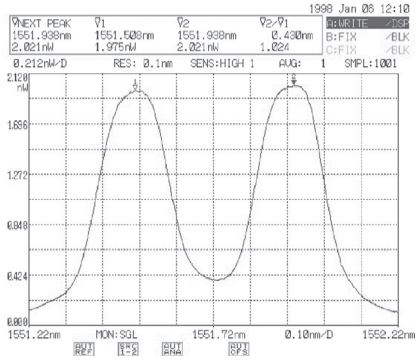

If a transverse force is applied along the axis p or q, then the relative strain field across the core changes, and the two spectral peaks will move together or apart in wavelength, depending on which axis is loaded, i.e., along one axis the relative strain difference across the core increases, and along the orthogonal axis the relative strain difference decreases.

The difference in wavelengths between the two peaks is directly proportional to the transverse strain.

It is also possible to measure three axes of strain and three axes of strain plus temperature. This can be done by writing two fiber gratings at different wavelengths at the same location. The result is four spectral peaks that form a 4×4 matrix that can be solved for the three strain axes and temperature.

Bragg Grating Pressure Sensor

When a Bragg grating is written onto an optical fiber, it can be used as a **pressure sensor**. In the simplest case, the fiber grating may be written onto a conventional single-mode optical fiber. When the fiber is exposed to pressure, it is under compression, and there is a shift toward short wavelengths. This shift is small compared to that induced by temperature changes such that effective pressure sensors of this type require extreme temperature compensation.

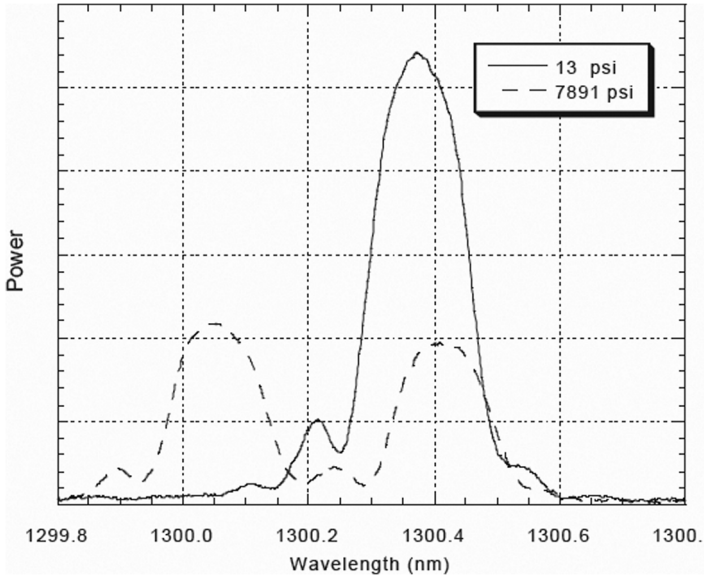

There is another, much more effective way to implement a fiber Bragg grating pressure sensor based on a side-hole optical fiber. In this case, the optical fiber is constructed in a manner similar to a conventional single-mode optical fiber, but two air holes are placed around the core. The above figure shows an example with a 125-μm-diameter optical fiber and a 30-μm side hole. When pressure is applied, the result is differential stress across the core. The spectral peak-to-peak separation is proportional to the pressure only, and the overall spectral shift can be used to simultaneously measure temperature.

Fiber Etalon Theory

The **Fabry–Pérot etalon** consists of two inline mirrors. The mirrors generate a resonance condition when there are an integral number of wavelengths between them, and the pair becomes transparent at that wavelength. At wavelengths that are off resonance, the transmission depends strongly on the reflectivity of each mirror.

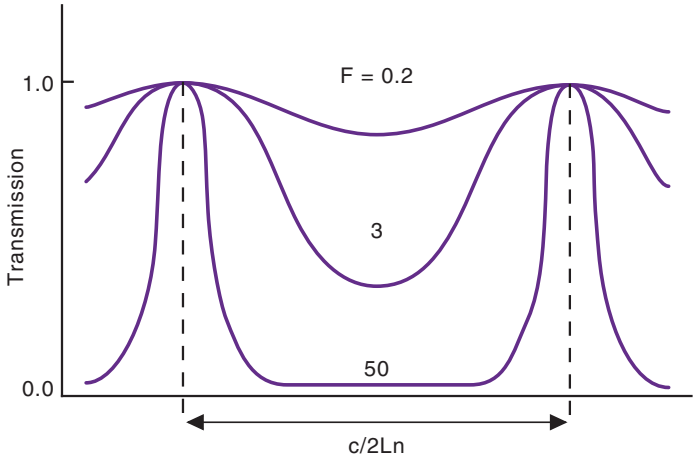

The **finesse** F of a pair of mirrors of equal reflectivity R is given by

$$F = 4R/(1 - R)^2$$

The higher the reflectivity is, the sharper the peaks, as illustrated by the figure. The fiber etalon can be used as a sensor in combination with a spectral read-out unit that is capable of measuring the position of the peaks. Alternatively, the fiber etalon can itself be used as a spectral measurement device. When the spacing L between the two mirrors changes, the **free spectral range**, given by $c/2Ln$ (where c is the speed of light and n is the index of refraction between the two mirrors), shifts. This behavior allows a narrow transmission passband to be scanned, which is commonly used to support fiber grating systems.

Fiber Etalon Sensors

There are two principal types of single-mode **fiber etalon sensors** that have been employed. The first includes **intrinsic** fiber etalon sensors, wherein a single-mode fiber is cleaved and a reflective material (that may be a dielectric coating) is applied to the core of the fiber. This product is then fusion spliced to a second optical fiber to form a mirror internal to the fiber itself. A variant approach uses one internal mirror and a second on the end of the fiber to form an etalon sensor.

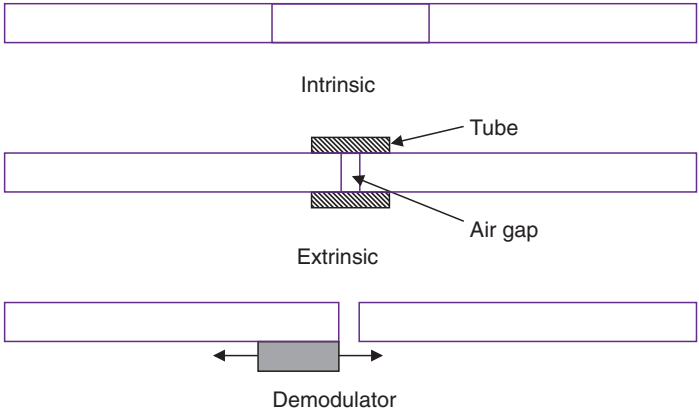

The second type involves putting mirrors on the end of the optical fibers and inserting them into a capillary tube. There is an air gap between the two mirrors, which has the advantages of minimizing thermal and polarization issues. The principal disadvantage of this approach is that the overall diameter of the sensor has been increased beyond the diameter of the optical fiber.

The third diagram of the figure illustrates a fiber etalon used as a spectral scanner. This can be used to support both types of fiber etalon sensors by matching transmission windows to read out the effective cavity length of the fiber etalon sensor and, in turn, the environmental effect inducing that length.

Time Division Multiplexing

After an appropriate fiber sensor has been selected for an application, an important consideration is how to minimize the cost and complexity of the read-out system and the sensors. Multiplexing is one of the key advantages of fiber sensors because the intrinsic bandwidth allows many sensors to be supported along a single fiber line. One of the most commonly used multiplexing techniques is **time division** (or domain) **multiplexing** (TDM).

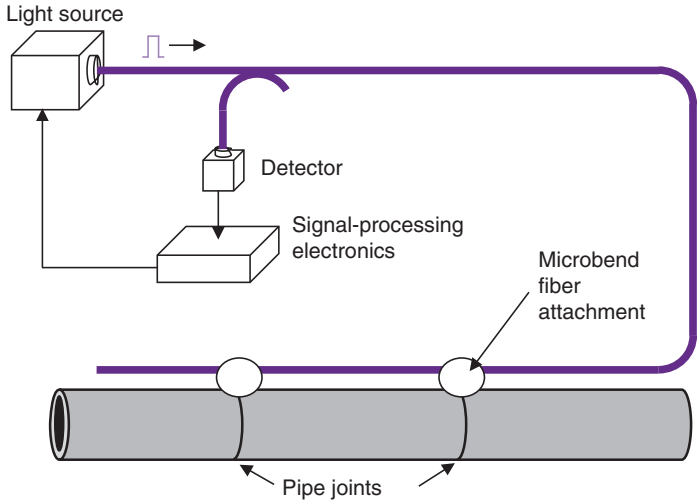

In this case, a short pulse of light is directed into an optical fiber and propagates to a series of sensors that change some property of the light beam (e.g., amplitude, polarization, phase, or frequency) and reflect the signature back on the optical fiber or an adjoining one to a detector and signal processes. Successive light pulses are separated out in time because the sensors are spatially displaced such that each signal can be separated out in the time domain. One limitation of this approach is that the spatial separation of the sensors is limited by the time resolution of the system.

Wavelength Division Multiplexing

One method to overcome the spatial limitations of **TDM** is to utilize **wavelength division multiplexing** (WDM). In this case, each of the inline fiber sensors is wavelength encoded with a distinct wavelength that is continuously monitored by the read-out system. A natural example of a fiber sensor that can easily be used with this method involves fiber gratings wherein the period is adjusted such that a distinct, separable wavelength is reflected.

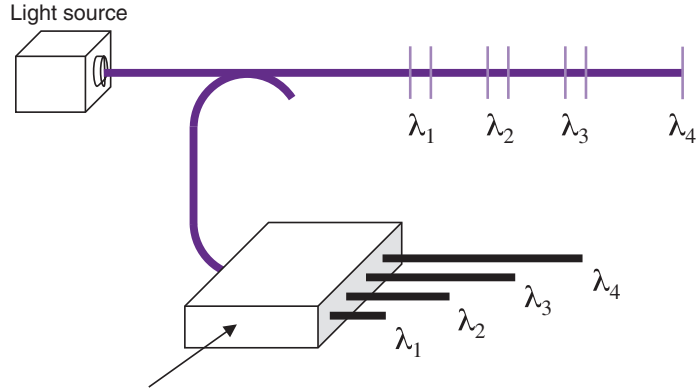

The WDM technique can also be integrated with a TDM system to support many more inline sensors. For example, a TDM sensor may have the ability to separate out sensors provided the spatial separation is one meter. The application, however, might require that fiber sensors be placed every 10 cm. Clusters of ten sensors supported by the WDM method with 10-cm spacing can then be used every meter to significantly enhance the number of sensors supported. The reflectivity of each cluster of sensors must be adjusted (lowest reflectivity first in line, highest last) to optimize performance.

As a practical matter, the number of shaded clusters is usually limited to less than ten. Other multiplexing methods can extend the number of sensors.

Optical Frequency Domain Reflectometry

It is possible to multiplex hundreds of weakly reflecting fiber gratings at the same wavelength by using a multiplexing technique known as **optical frequency domain reflectometry** (OFDR). In this case, a fiber grating may be written at low cost as a fiber is pulled on a draw tower with reflectivity on the order of a hundredth of a percent. This arrangement avoids the problem of multiple reflections generating unwanted signals. A tunable laser is used to scan out a wavelength range wide enough to support the specific application needs (e.g., minimum and maximum strain measurements). A Michelson interferometer configuration is used, where one leg contains the weakly reflecting fiber gratings and the other contains a reference reflector.

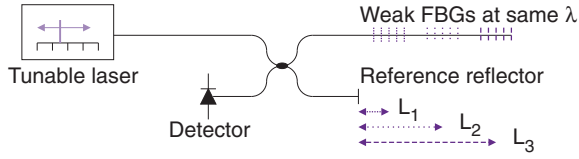

$$I_D = I_0 + I_1 + 2\sqrt{I_0 I_1}\sin\left(\frac{4\pi nL}{\lambda}\right) + \ldots \qquad f_D = \frac{2nL\, d\lambda/dt}{\lambda^2}$$

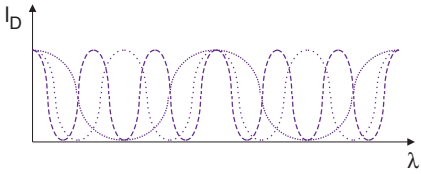

Digital filters used to pick out individual grating profiles.

As the laser is scanned, the difference in length between the first fiber grating and the reference reflector establishes a carrier frequency for the first fiber grating. This is different for each of the inline gratings and allows them to be separated in the frequency space. After they are separated using a Fourier transform, the wavelength associated with a particular inline fiber grating can be separated out using an inverse Fourier transform process. The computational requirements are high, resulting in a lower bandwidth than WDM can support, but it has the distinct advantage of supporting hundreds of high-spatial-resolution measurements.

Frequency Division Multiplexing

Frequency division multiplexing (FDM) can be used effectively to support arrays of Mach–Zehnder and Michelson interferometers. In this case the light source is operated in a chirped mode where the frequency of the light output changes at dF/dt. By arranging each successive fiber interferometer to have a net path length difference $(L - L_m)$, the two light beams will combine after exiting the interferometer with a carrier frequency F_m given by

$$F_m = (L - L_m)n/c$$

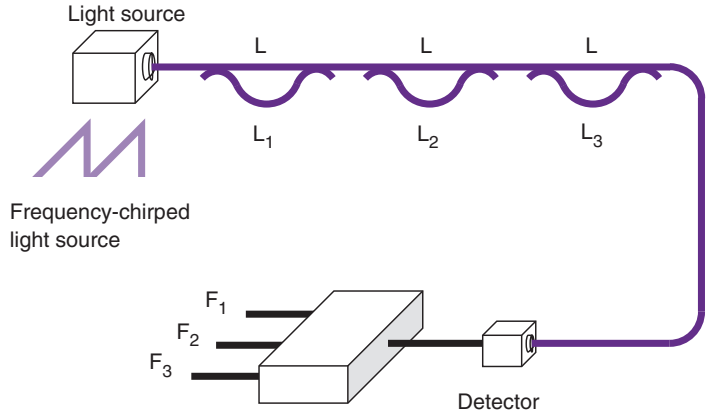

The frequency signal associated with each of the length offsets is then used to separate out each of the successive signals from the Mach–Zehnder (transmission) or Michelson (reflection) interferometers.

One key limitation of this approach is that its performance is highly dependent on the stability of the light source. In particular, if the frequency of the light source varies in a random manner, the offset between the legs of the interferometer generate corresponding **phase noise** $d\phi = 2\pi dF(L - L_m)n/c$.

Coherence Multiplexing

Coherence multiplexing is a technique that may be effectively used to support a relatively small number of fiber sensors. Typical applications involve interferometers that have two offset path lengths, including the Mach–Zehnder and Michelson interferometers and the Fabry–Pérot etalon operated in reflection.

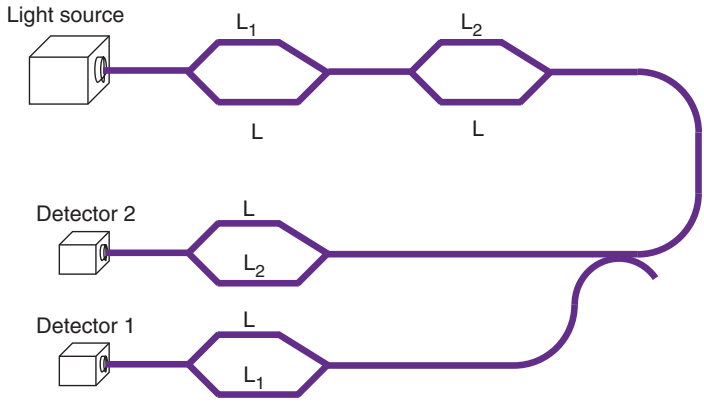

A light source is chosen with a coherence length that is short with respect to the path length difference between the two legs of the interferometer being multiplexed. Each successive interferometer is arranged such that the difference in the net optical path length [$(L_1 - L_2)$ in the illustration] is again much longer than the coherence length of the light source.

An output detector is designated for each interferometer, and in front of it there is a compensating interferometer that specifically offsets that difference in path length associated with the sensor.

Note that there is a significant loss associated with the multiple paths associated with this technique; thus, it is usually used to support small numbers of sensors (one to four) at one time.

Spatial Multiplexing

Another multiplexing method, known as **spatial multiplexing**, uses an array of light sources modulated at a frequency ω_m that is used to support J lines of sensors. The output from each of these lines is directed to K output detectors. The idea is that each of these detectors has a system of electronics behind them that are capable of separating out the J carrier frequency. In this way, J lines in and K lines out support JK sensors.

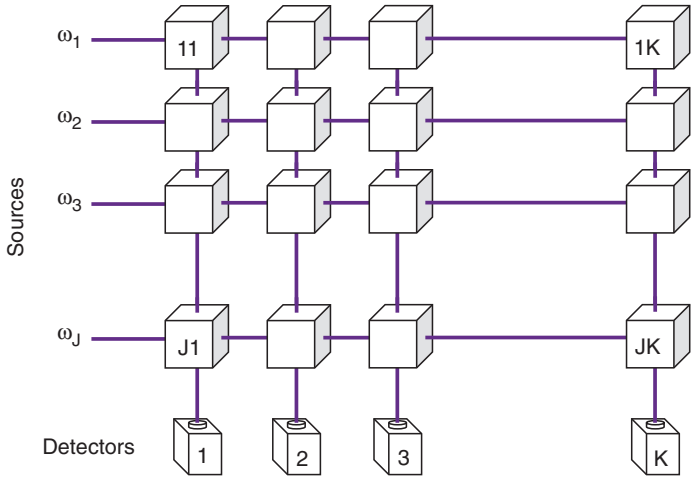

The principal application area of this type of multiplexing involves very-low-cost sensors. In particular, if the light sources are amplitude modulated and each of the fiber sensors is a low-cost, modest-performance amplitude sensor, then this may be an effective multiplexing technique for a specific application, e.g., microbend sensors woven into a structure where it is desirable to locate the position of a disturbance continually.

The disadvantage of this approach is the relatively high number of input and output fibers involved.

Distributed Raman Sensor

The designer of fiber sensor systems often faces the problem of isolating undesired environmental effects with the objective to measure one or more specific environmental parameters and be immune to all others. The **distributed Raman sensor** has the great advantage that it is sensitive only to temperature. When a fiber changes temperature, it excites vibrational modes within the fiber structure itself. When a short light pulse is directed down the optical fiber, there is a small amount of backscattered light due to losses in the optical fiber.

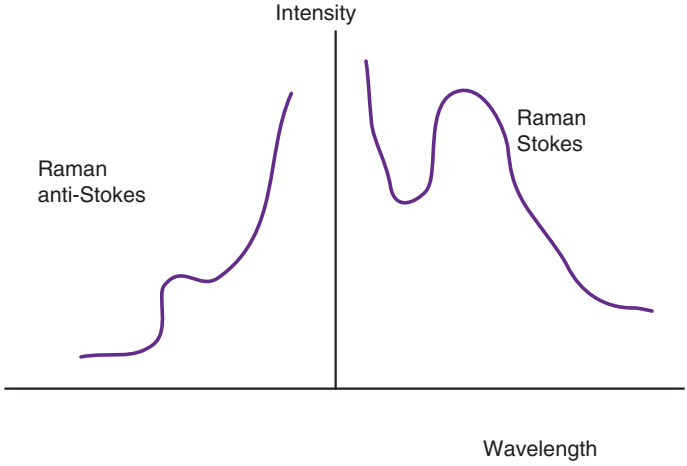

The backscattered light from each region that is resolved by TDM has a component that is upshifted in frequency; the photons absorb a phonon associated with the vibration of the fiber (**anti-Stokes**) and a component associated with the photons converting a portion of their energy into phonons (**Stokes**). The terms are designated as such because Stokes believed that energy from the photons could only be converted into vibrational phonons. The ratio of Stokes to anti-Stokes backscattered light is proportional only to temperature.

Distributed Brillouin Sensor

The **distributed Brillouin sensor** features a laser source that generates pulses of high-coherence light that when they propagate down an optical fiber generate both Stokes (longer wavelength) and anti-Stokes (shorter wavelength) side bands, just as in a distributed Raman sensor. Unlike the Raman version, these side bands are very narrow spectrally because they are generated by the bulk movement of molecules acting in concert, rather than individually.

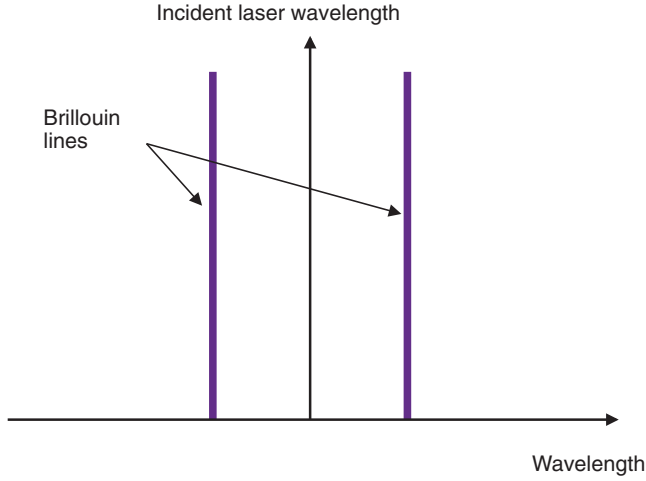

The scattering is generated by the product of a moving diffraction grating from the light beam internal to the fiber and the resulting refractive-index variations caused by acoustic waves propagating longitudinally along the fiber axis. This situation results in quantized Doppler shifts, where the resulting side bands are photons that add or subtract the energy of a phonon associated with the acoustic wave, an action similar to that of an acousto-optic modulator. These side bands are very narrow and have a much stronger reflectivity than a Raman sensor, so a distributed Brillouin sensor relies more on electronic processing and has a better SNR, allowing for greater range.

Brillouin Distributed Sensor Capabilities

The **distributed Brillouin sensor**, as discussed earlier, generates narrow frequency-shifted side bands. The Stokes (downshifted) and anti-Stokes (upshifted) photons are displaced in frequency by plus or minus

$$\upsilon b = 2n\, v_a/\lambda_p$$

where n is the index of refraction of the optical fiber, v_a is the acoustic velocity, and λ_p is the frequency of the pumping laser.

There are two types of distributed Brillouin sensor: those based on spontaneous and stimulated emission. For lower-power laser pumping, the acoustic waves are generated spontaneously, but if the power is increased, the acoustic waves will interact with the laser pump light and become much stronger, moving into the stimulated regime. This behavior allows for larger signals and longer distributed sensors, moving from 30 km toward 50 km. The spontaneous Brillouin system has the advantage that it can be used to measure both strain and temperature along the distributed length instead of just one parameter.

In particular, the Brillouin frequency shifts for temperature and strain are given by

$$F_T = 1.1\,\text{MHz}\,(\text{K}^{-1})$$
$$F_\varepsilon = 48\,\text{kHz}\,(\mu\text{strain}^{-1})$$

The key to measuring both the temperature and strain simultaneously is to recognize that there is a power-level dependence of the frequency shift as a function of the temperature and strain. These coefficients are given by

$$P_T = -7.7 \times 10^{-4}\%\,(\mu\text{strain}^{-1})$$
$$P_\varepsilon = 0.36\%\,(K^{-1})$$

They allow for the generation of well-conditioned equations that can be inverted.

Distributed Sagnac Sensor

The **distributed Sagnac sensor** relies on the response of the Sagnac interferometer to a time-varying environmental effect that is zero at the center of the Sagnac loop and increases as the location of the effect moves toward the central beamsplitter.

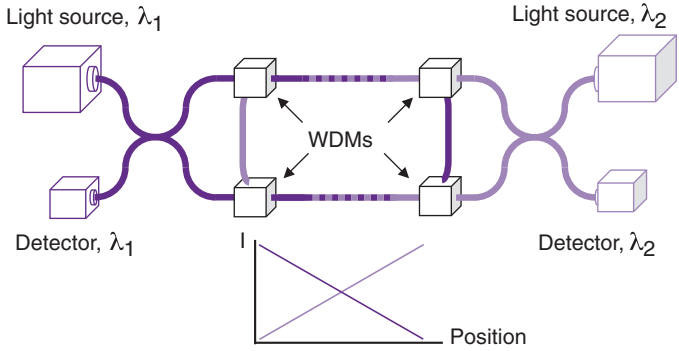

In order to measure both the location and amplitude of a time-varying environmental event, two interlaced Sagnac loops are necessary. The sum of the two signals allows the amplitude to be measured, and the ratio allows the position.

One of the advantages of this approach is that it can use low-cost components. The light sources can be low-coherence LEDs, and the WDM elements can be conventional fused fiber couplers. The operating wavelengths for the Sagnac loops can be 1300 nm and 1550 nm, utilizing the two major telecom wavelength bands.

Because low-coherence light sources are used, backscatter and cross-coupling between the loops is not an issue.

This approach is limited to time-varying events because the response of the sensor to low frequencies falls off at a rate that is proportional to the frequency of the signal.

Distributed Sagnac–Mach–Zehnder Sensor

The **distributed Sagnac–Mach–Zehnder sensor** relies on the response of the Sagnac interferometer, which has no response to a time-varying effect in the center of the Sagnac loop and has increasing response as the environmental effect moves toward the central beamsplitter. In this case, a leg of the Mach–Zehnder is integrated into the distributed sensing region of the Sagnac loop via WDM elements.

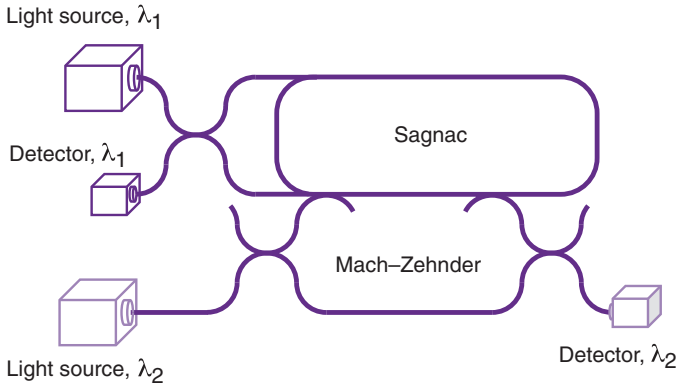

The response of the Mach–Zehnder in this region is flat over the entire length such that it can be used to measure the amplitude of the environmental effect. The Sagnac interferometer response is position dependent with respect to a time-varying environmental signal. Taking the ratio between the Mach–Zehnder signal and the Sagnac signal can be used to locate the event.

The distributed Sagnac–Mach–Zehnder sensor utilizes two different types of light sources—a low-coherence light source for the Sagnac and a long-coherence light source for the Mach–Zehnder—which can increase the price of the system and cause difficulties associated with isolating noise sources. In particular, the long-coherence light source, if there is cross-coupling into the Sagnac loop, will generate noise due to coherent backscatter, and there is an issue associated with optical isolation of the laser.

Sagnac Secure-Communication System

A **Sagnac interferometer** can be used to support high-speed secure communication, and this implementation can also be used to measure a portion of the length of the Sagnac loop with high accuracy. The basis configuration consists of a low-coherence-length light source that generates counter-propagating light beams in a Sagnac loop. A phase modulator that can be a very-high-speed integrated optic modulator is placed in a transmitter region offset from the center of the Sagnac loop. To transmit data, short phase pulses are injected into the system and propagate in both directions. The offset length of the loop may be measured by adjusting the frequency of the input pulses until they exactly overlay.

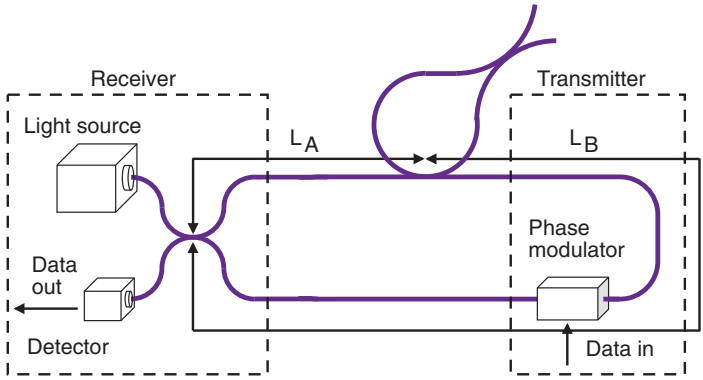

The time delay is proportional to the length. In **secure-communication mode**, the data is injected into data packets and received when the two counterpropagating light beams combine at the central beamsplitter. An intruder tapping into the system would see what looks like a continuously-on light source without data. A more-sophisticated intruder might try to build a compensating interferometer. The Sagnac interferometer is automatically matched while the intruder faces matching a very long, two-leg interferometer. This can be made more difficult by adding alarms that measure the amount of power being tapped and by placing a random path length generator in the center of the Sagnac communication loop.

Low-Coherence Strain-Sensor System

One of the earliest implementations of **strain sensors** associated with monitoring bridges, buildings, dams, and other civil structures was the SOFO sensor developed by Smartec (see figure, courtesy of Smartec). In this case, a Michelson-interferometer-based sensor was constructed by placing a coupler in a tube along with the two legs of the coupler, where one leg is constrained and the other is collocated to provide temperature compensation. The tube can have lengths that range from a fraction of a meter to several meters. When the tube is buried in a civil structure, it moves with the structure, and the relative lengths of the two light beams change.

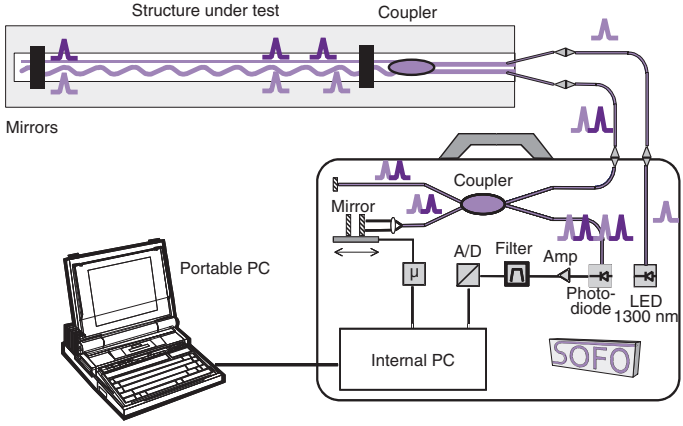

A low-coherence-length light source, originally an LED, illuminates the sensor, and the combined beams are offset in pathlength and only interfere when passed through a compensating interferometer (consisting of another Michelson interferometer with a scanning mirror). When the two legs are matched within the coherence length, interference fringes appear, and the peak is determined to measure the absolute length of the fiber sensor.

By using a fiber grating sensor placed in a tube and anchored at both ends, similar performance can be achieved; a loose grating can be used for temperature.

Civil Structure Applications

Fiber sensors may be used to support a wide variety of **civil structure applications**, including measuring the structural integrity of buildings, bridges, dams and tunnels. Many of these implementations rely on tubular structures, embedded into concrete and often attached to rebar, to measure strain on an optical fiber under tension. Another approach embeds the tubular structures in composite materials that are used to reinforce beams in a bridge or building. The tubular approach has also been successfully used to embed strain sensors in freeways to measure the weight and speed of traffic.

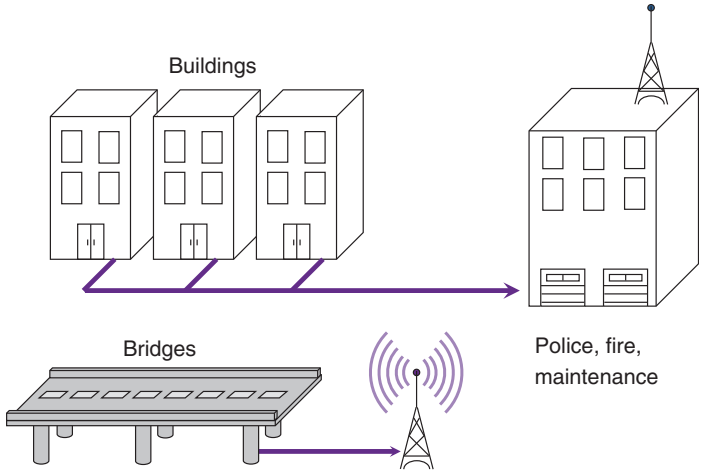

In addition to strain, temperature is sometimes measured, often to compensate for thermally induced changes to the structure. The other major area under development for civil structures involves fiber optic sensors to measure corrosion. These measurements are usually either

- based on changes to chemical properties that are measured by evanescent fiber sensors or
- they rely on strain field changes induced by fiber sensors that are embedded in or attached to metal structures.

As the metal corrodes, the axial and/or transverse strain-field changes, providing an indication of the degree of corrosion.

Damage-Assessment Microbend Sensor

Even the simplest fiber optic sensors can be used to support important functions. The following figure illustrates a configuration that can measure and localize damage to a structure. In this case, light sources, such as low-cost LEDs, are used to couple light into arrays of microbend-sensitive fiber that are woven into or attached to the structure. When an impact occurs that induces damage, the structure is deformed, and microbend loss changes the light level detected for that specific fiber element. By using 2D configurations, the location of the damage may be determined.

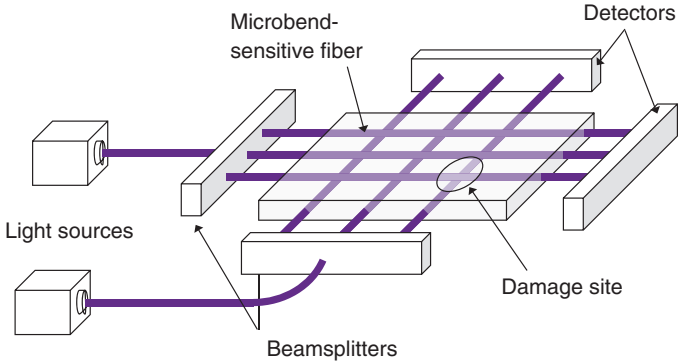

This configuration can also enable safety mats for use with dangerous machinery. Microbend-sensitive optical fibers are woven into the mat, and when an operator is too close to the machinery and steps on the mat, the signal level goes down, and the machinery is switched off. For this simple application, only one light source and detector is needed. The microbend-sensitive optical fiber is wound back and forth through the mat as a single strand.

Another variant of this approach uses metal plates with a specific period optimized for the maximum microbend response for an optical fiber design. Pressure on the plate changes the amplitude output.

Position Sensors

Flight-control systems require accurate reading of rotary and linear position associated with the wing and tail flaps. One of the first implementations of fly-by-light involved these types of fiber sensors, which are based on reflective surfaces. An optical fiber is positioned so that light exiting the fiber hits the region where there is either a reflective or dark surface. When the light reflects from the surface, the detector and associated electronics record a one or zero.

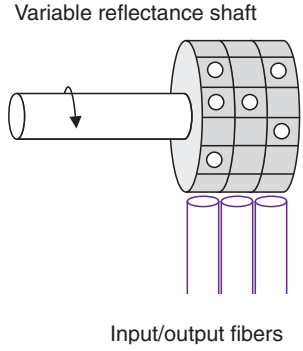

Each position is digitally encoded around the surface of a cylinder of flat card. In addition to one-to-one **position sensors**, there are implementations that use WDM and TDM.

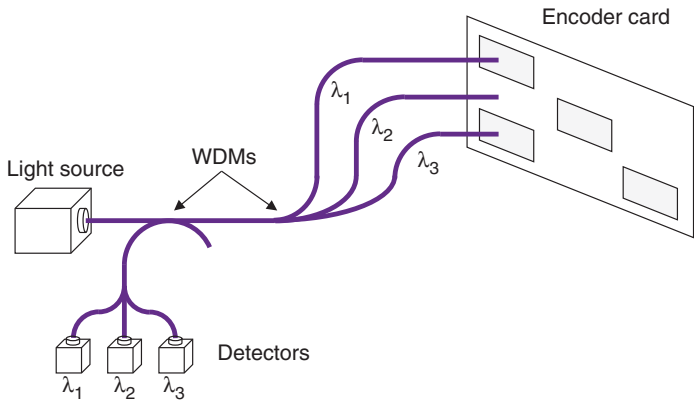

Smart Bed

Optical fiber modal domain sensors can be used for intrusion detection and various other applications. In particular, the medical community is interested in them as the transducer mechanism for the so-called "**smart**" **bed**. In this case, the optical fiber sensor is placed beneath the mattress of a patient's bed so that any movement of the patient due to body motion, breathing, or heartbeat perturbs the mattress, which perturbs the fiber and produces a measureable signal.

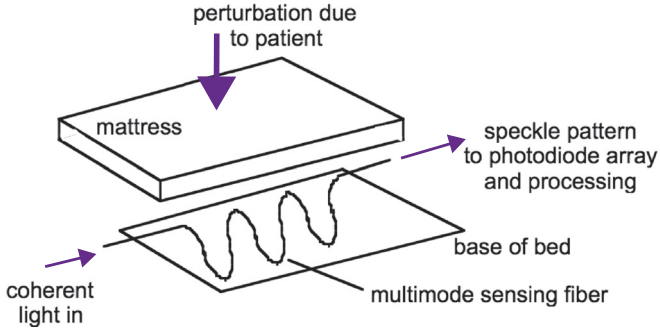

The smart bed can determine an indication of a patient's **breathing rate** and **heart rate** without any intrusive attachment to the patient's body. The following results show that the patient

(a) moves to the edge of the bed,
(b) gets out of bed,
(c) moves away from the bed,
(d) sits down on the edge of the bed,
(e) settles down in bed, and
(f) makes small movements in bed.

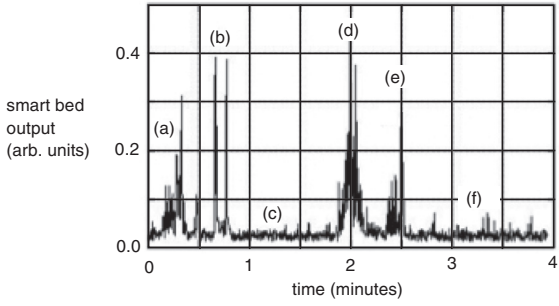

Catheter Shape Sensing

Robotic surgery entails the use of a robotic catheter operating within the body, directed by a surgeon adjacent to the patient. The position of the catheter is monitored via low-level x-ray images taken continually during the surgery. The use of x-rays necessitates that the surgeon wear heavy, protective lead clothing; even so, after a number of years, these surgeons display increased rates of cancer. For that reason, alternate methods of locating robotic catheters within the body have been developed, including one that uses a specialty fiber containing three single-mode cores that have arrays of low-reflectivity Bragg gratings (1-cm gratings separated by 1 cm) written into them.

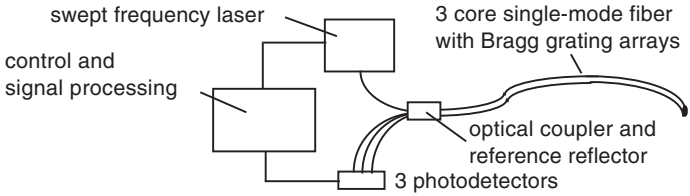

Light from the **swept frequency laser** is coupled into each of the fiber cores, and the backreflected light from each core is captured by one of three photodetectors. The three return signals are then mixed with the real-time frequency of the laser source at the reference reflector. The **beat signals** from all of the Bragg gratings in the array are superimposed in the time domain. They are separated through a **Fourier transform—windowing**—inverse Fourier transform process, such that the wavelength of the light reflected by each grating in the array can be determined, and thus the strain seen by the grating can be quantified. Processing this data allows for the calculation of the spatial curvature of the fiber at any point. Sequentially adding these curved sections then maps the shape of fiber in three dimensions and thus the shape of the catheter into which it is integrated.

Radiation Dosage Sensing

Neutron detection using lithium-6 glass was first demonstrated in the late 1950s. Pacific Northwest National Labs incorporated this technology into scintillating optical fibers in the 1980s and 1990s and licensed the technology to Oxford Instruments (and later Nucsafe).

The lithium-6 is incorporated into cerium-enriched optical fibers. When a thermal neutron interacts with lithium-6, it generates a tritium ion, an alpha particle, and kinetic energy. The alpha particle and tritium ion interact with the cesium-3 ions in the optical fiber structure, forming an excited state that decays into photons in the range of 390–600 nm. The several thousand photons emitted per event are detected as a flash event and used to measure **radiation dosage**.

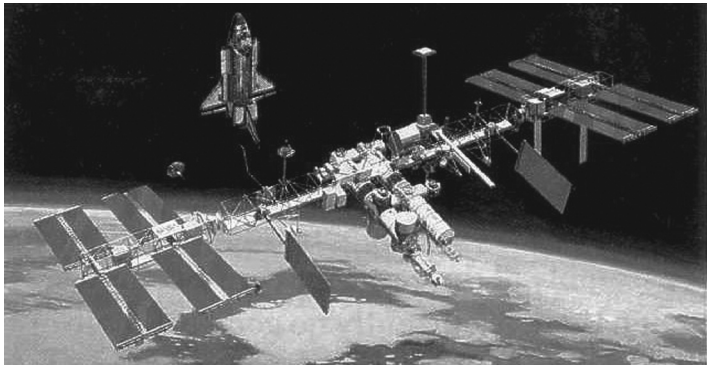

There are other types of radiation, e.g., those that affect space flight. In this case, gamma radiation plays a role, as do particle storms generated by the sun. Experiments have been performed by NASA to evaluate the changes in optical fiber attenuation for long-duration missions. A silica-based optical fiber that has a pure silica optical core and fluorine-doped cladding changes much more slowly than germanium-doped optical fibers. If fibers are selected that have different ratios of attenuation with radiation, then effective, long-duration radiation-dosage sensors can be designed for space.

Proximity Fiber Sensors

There are situations where it is important to know whether or not a door is closed, e.g., on a ship or submarine. If the hull is breached or there is a shipboard fire, it is critical to know that containment doors are properly shut and sealed. When light is directed into a fiber exit, it spreads, and if a second fiber is placed nearby, the amount of light it captures depends on the distance between the fibers. This type of arrangement can be used to support simple **proximity** and **closure sensors**.

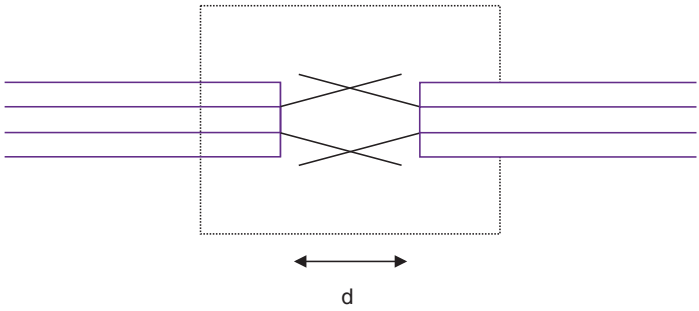

Another approach uses one or more fibers in combination with a mirror. As the mirror moves back and forth, the amount of backcoupled light varies. This principle can be used for a door closure with a reflective surface or for a vibration sensor for a flexible mounted mirror.

A fiber optic liquid-level measurement system is a variant wherein a bare fiber end reflects light back until the fiber is dipped in a liquid (often water) and the reflection drops to zero. This is commonly used to measure the depth of water wells.

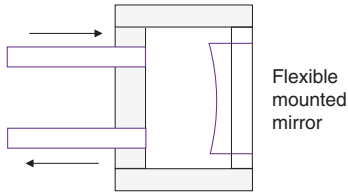

Oil and Gas Applications

There have been major investments by the oil and gas industry to take advantage of the capabilities of fiber optic sensor technology. For **oil and gas pipelines**, distributed fiber optic sensors have been used to identify and localize leaks. (An important example is the Alaska pipeline.) The oil is preheated before insertion into the pipe; if oil leaks on any section of the pipe, the temperature rises and can be detected. A single Brillouin distributed-strain-and-temperature-sensor read-out unit can support this type of monitoring over a span of 100 km (50 km in each direction).

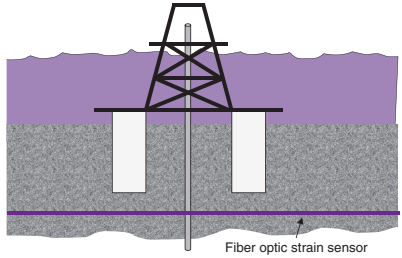

For downhole applications, it is important to measure pressure and temperature. This improves the safety of the well and allows more efficient extraction of oil, easily paying for the system. Raman distributed sensors can support downhole temperature measurements, and a series of fiber optic pressure sensors have been developed for this purpose. Acoustic arrays based on the Michelson and Mach–Zehnder interferometer permit exploring for oil and gas via surface ships. More recently, they have been used downhole to support exploration and extraction operations from existing oil and gas wells. This application is particularly important for oil and gas fracking operations. The objective, again, is to improve the safety and efficiency of operations, with the added benefit of identifying oil pockets.

Strain Imaging and Monitoring Composite Materials

Fiber optic strain sensors can be embedded into composite structures and used to monitor both strain and temperature during cure. In particular, if fiber grating sensors are embedded into **composite materials**, their wavelength will shift as temperatures rise toward longer wavelengths. When organic composite materials start to cross-link during cure, the pressure exerted on the fiber grating will move them toward shorter wavelengths, and the onset of cross-linking can be tracked. A shift in the overall strain profile after cure can be used to support the modeling of residual strain internal to parts and their inherent strength.

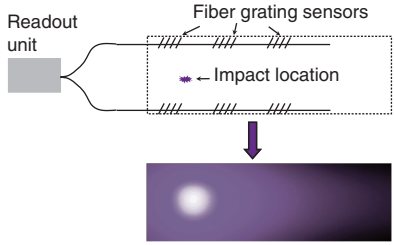

If arrays of fiber gratings are embedded into a composite structure and an impact occurs that results in internal damage, the strain-field changes can be measured by the fiber gratings and used to localize and determine the magnitude of the damage. This approach to damage assessment is called **strain imaging**, and it offers a competitive alternative to ultrasonic and eddy-current methods. Both single- and multiaxis fiber grating strain sensors may be employed. The multi-axis sensors allow measurements in both the in-plane and out-of-plane directions. Another important application involves using fiber gratings to monitor strain changes in adhesive joints, enabling an assessment of the health of the joint and modeling of predictive failure.

Plastic Optical Fibers

Most fiber optic sensors are fabricated using silica-based optical fibers, but **plastic optical fibers** offer the possibility of very-low-cost alternatives. They are widely used for low-cost communication interconnects, as shown below.

Most of the early plastic fibers were made of acrylic cores with fluorinated polymers for the cladding. More recently, there has been a shift toward lower-loss perfluorinated polymers. The immediate benefit of plastic optical fibers is for applications that require the lowest possible cost and have modest performance requirements, e.g., on/off door-closer fiber sensors and angular- and linear-position sensors. These types of fiber sensors require large-core multimode sensors and involve short distances. Although plastic optical fibers are capable of supporting links on the order of 100 m, distances longer than that quickly move toward silica-based fibers.

There has been some work done on writing fiber Bragg gratings into plastic optical fibers, which could have advantages for applications requiring wide strain ranges. Deformation of these fibers remains an issue.

Integrated Optics

Fiber optics can be combined with **integrated optics** devices that can be used to direct, modulate, and control the polarization of light beams. These devices can be formed in **lithium niobate**, and the local index of refraction can be controlled by proton bombardment; although other processes are possible, this one tends to preserve only one polarization state. This type of device can be configured to act as a polarizer, beamsplitter, and (because lithium niobate is an electro-optic material) a modulator. The result is that many of the components necessary to support a fiber gyro other than the light source, detector, and optical fiber interconnects can be formed on a single chip.

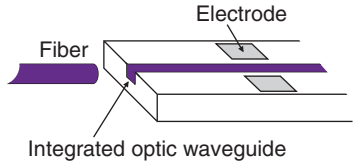

Because the polarizer on the chip may not be of sufficiently high quality, an external fiber polarizer might also be required.

The integrated optics chips can be formed into Mach–Zehnder interferometers. A long-coherence-length polarized light source can be coupled to the chip and a phase modulator put in one leg (or both legs operated differently) to induce phase differences that can be used to modulate the amplitude of the optical output beam. Another common application is to phase ramp a phase modulator in front of the highly coherent, stable light source to induce a very-well-controlled frequency ramp or offset that can be used in interferometeric and distributed sensors.

Fiber Light Sources

Fiber light sources can be used in applications that require high power and, in some cases, unique spectral properties. The basic configuration consists of a pump laser diode, a WDM coupler, and a section of optical fiber that is doped with an active material that absorbs photons from the pump laser and emits at a specific wavelength.

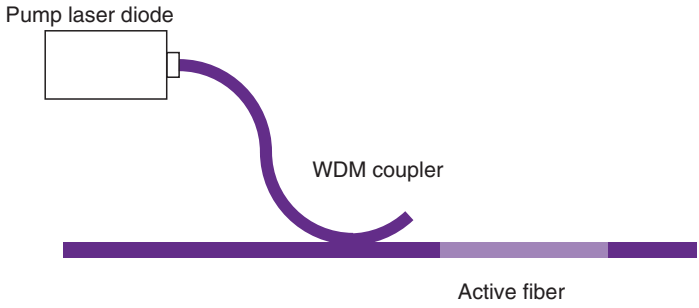

The most common case is a pump laser with a 980-nm laser diode that couples into a 980-nm/1550-nm WDM coupler. The 980-nm light is absorbed by erbium sites in a single-mode optical fiber, such as a Corning SMF-28 single-mode-optical-fiber-like structure, doped with germanium and erbium.

The higher-energy 980-nm photon decays into a lower-energy 1550-nm photon via spontaneous emission if there are no provisions for mirrors around the active fiber. The result is an effective high-power, completely depolarized light source that can be used very effectively in many fiber sensor systems, especially those that are based on a fiber grating.

Other wavelengths are possible by changing the wavelength of the light source and dopant materials for coverage in both longer and shorter wavelengths. Using a neodymium-doped optical fiber to support a 1.06-μm stable source for fiber gyros is an important example.

Polarization-Preserving Optical Fibers

For interferometers that involve combining light beams from two separate optical paths, it is necessary to ensure that the polarization of the light beams is controlled to avoid signal fade out (where the two beams are orthogonally polarized). It is often highly desirable to have the light beams combine with the same polarization state; this often results in the highest possible sensitivity and accuracy. **Polarization-preserving optical fibers** have been devised to accomplish this.

There are a number of different types of polarization-preserving optical fiber. The most commonly used types have fiber structures that are based on hard and soft materials placed in the cladding that induce stress differences in orthogonal directions across the fiber core. Another structure uses fibers with elliptically shaped optical cores and also has an effective index of refraction difference in the two orthogonal directions. Because it does not have internal stress induced by different materials, it is mechanically more stable, and a side can be ground off to form a D-shaped fiber that is useful for some applications that require physical orientation. By designing one of the two orthogonal polarization states to have high loss with bending, fiber polarizers can be designed that are of particular interest to fiber gyro (rotation) sensor applications where the polarization of the counterpropagating light beams must be precisely matched to produce the highest performance.

Fiber Depolarizer

There are two issues associated with **polarization-preserving optical fibers**:

- They are much more costly than conventional single-mode optical fibers, and
- The components needed to use a polarization-preserving optical fiber in an interferometer are also more expensive, and the process to connect the orthogonal axes with proper orientation is more difficult.

There is another approach that is useful with interferometers that utilize low-coherence light sources and have large optical path lengths, the principal example being the Sagnac interferometer. In this case, a **fiber Lyot depolarizer** may be used.

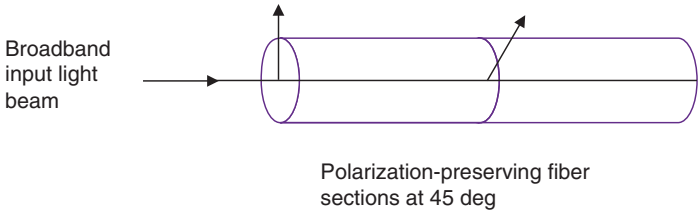

The device is formed by splicing two lengths of a polarization-preserving optical fiber with their axes aligned at 45 deg with respect to each other. When a broadband light source, e.g., a LED or a broadband fiber light source with a spectral range of about 50 nm, and a typical commercially available polarization-preserving optical fiber are used, the fiber lengths are on the order of 0.5–1.0 m. The optimal length of the fibers can be adjusted. Longer lengths are required for light sources with narrower spectral range.

When the fiber depolarizer is placed in front of a polarized broadband light source, the fiber depolarizer converts each wavelength to a different polarization state such that, on average, for a two-leg interferometer, 50% of the light will recombine in the correct polarization state, thus trading loss for a lower overall system cost.

Manually Scribing and Breaking a Fiber

Although there are numerous automated, semi-automated, and manual tools available to **scribe** and **break** optical fibers, there are times (especially when building up a capability to develop fiber optic sensors) when a low-cost, manual method can be useful. For a glass optical fiber (either a glass core and cladding or a glass core with a hard plastic cladding), acceptable scribing and breaking can be performed by a rigid surface with an edge, some adhesive tape, a quantity of low-cost single-edge razors, and a silicon-carbide or diamond-edged scribe. The fiber is first taped to the rigid surface and held under tension with one hand while the other hand carefully cuts away the plastic around the fiber using the razor with downward strokes.

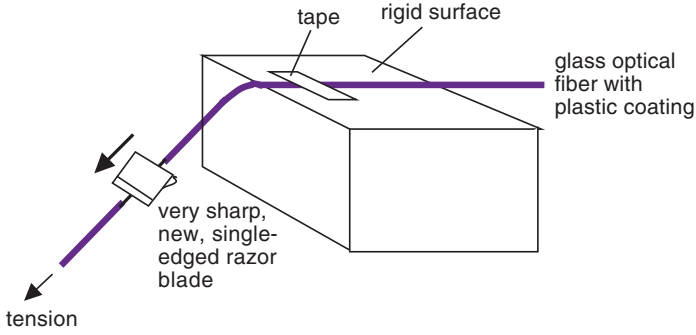

After the bare glass portion of the fiber is exposed, the fiber is held by the thumb and middle finger of one hand while bending the bare fiber in a slight curve around a portion of the index finger of the same hand. The other hand then scribes the bent section of bare fiber in a direction normal to the transmission axis. When done properly, this maneuver will leave a perfect glass-end surface.

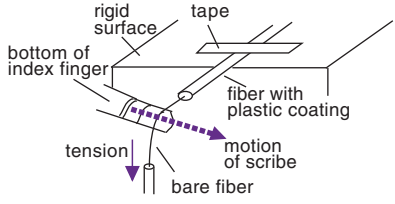

Using UV Curing Epoxy

An **ultraviolet (UV) epoxy** consists of liquid monomers and oligomers mixed with a small quantity of photoinitiators. When this mixture is exposed to intense UV light, it hardens very rapidly. The UV curing epoxies used in optical applications are also clear, uniform, and introduce minimal optical loss in the wavelength ranges of interest for fiber optic sensor development. Whereas more-conventional epoxies must be baked for significant fractions of an hour or more to cure, UV curing epoxies cure in seconds. Shown below is a plot of the fractional amount of cure for an acrylate material (polyol polyacrylate plus isocyanate functionalized polyurethane diacrylate).

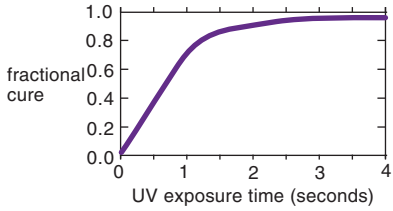

Rapidly tacking down optical components is one unique benefit of using an UV curing epoxy. It can also be used to rapidly create simple **splices**, as shown below.

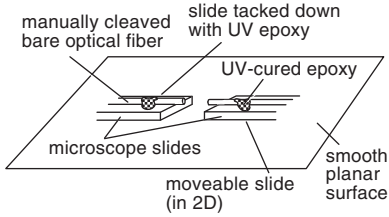

The moveable slide is adjusted so as to butt couple the two cleaved fiber ends, which are then bonded in place. Crude optical components, such as **semispherical lenses** on the ends of fibers, can also be created using an UV curing epoxy.

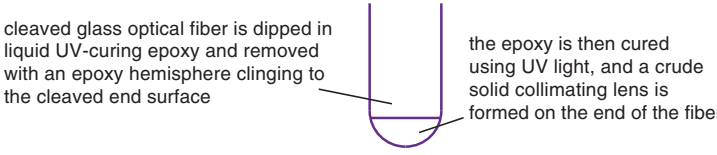

Experimental Use of a Lock-In Amplifier

When carrying out fiber optic sensor experiments, one of the first difficulties encountered involves variable ambient-light conditions. In particular, when fiber optic intensity sensors are involved, this problem can be so overwhelming that a lot of early research went toward eliminating any extraneous light. In effect, the researchers worked in the dark. A solution to this problem was quickly found though the utilization of **phase-sensitive detection** via a **lock-in amplifier**. A schematic diagram of a simple analog test setup employing this technique is shown below.

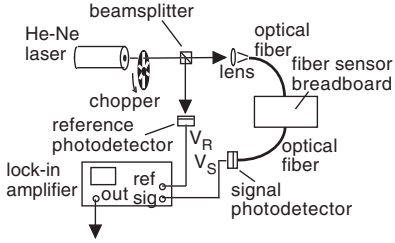

$V = A\langle V_S V_R \rangle_{dc}$ where A is a constant

In this example, light from a He-Ne laser is modulated by a mechanical chopper and then passed through an optical beamsplitter with one component detected and converted to voltage V_R by a reference photodetector. The other component is focused by a lens into an optical fiber, a fiber sensor breadboard, and a second fiber whose output is detected and converted to a signal voltage V_S. The reference voltage and signal voltages are then input to the lock-in amplifier, which provides a low-pass filtered average output proportional to their product. This dc output voltage V is proportional only to the amplitude of the component from the detected signal voltage whose frequency exactly equals the frequency of the reference signal, i.e., all detected signals due to ambient light conditions are rejected, and there is no need for darkness.

Equation Summary

Helmholtz equation:

$$\nabla^2 \mathbf{E}(\mathbf{r}, t) = \left(\frac{1}{c^2}\right) \frac{\partial^2}{\partial t^2} \mathbf{E}(\mathbf{r}, t)$$

Speed of light:

$$c = \frac{1}{\sqrt{\mu\varepsilon}}$$

Solution to the Helmholtz equation:

$$\mathbf{E}(\mathbf{r}, t) = \mathrm{Re}\{\mathbf{E}_0 \exp[i(\omega t - \mathbf{k} \cdot \mathbf{r} + \phi_0)]\}$$

Wave vector:

$$k = |\mathbf{k}| = \frac{\omega}{c} = \frac{2\pi}{\lambda}$$

Detected signal-to-noise ratio:

$$SNR = \frac{2(Ie\eta/hf)^2}{\left[3e^2(I + I_B)\eta B/hf\right] + 2ei_d B + (4k_B TB/R)}$$

Minimum detectable optical power:

$$I_{\min} = \frac{hf}{e\eta} \sqrt{\frac{2k_B TB}{R}}$$

Strain as a function of pressure:

$$\varepsilon = T_1(\varepsilon, P)P$$

Light phase as a function of strain:

$$\phi = T_2(\phi, \varepsilon)\varepsilon$$

Output intensity as a function of phase:

$$I = T_3(I, \phi)\phi$$

Output intensity as a function of pressure:

$$I = T_3(I, \phi)T_2(\phi, \varepsilon)T_1(\varepsilon, P)P$$

Equation Summary

Photovoltaic detector output:

$$V \cong A\ln\left(R\frac{I}{i_0}\right)$$

Photoconductive detector output:

$$i = i_0[\exp[(AV_B - 1)] - RI]$$

Snell's law:

$$n_1 \sin\theta_1 = n_2 \sin\theta_2$$

Lensmaker's formula:

$$\frac{1}{s_1} + \frac{1}{s_2} = \frac{1}{f}$$

GRIN lens transmission:

$$\begin{pmatrix} r_2 \\ \dfrac{dr_2}{dz} \end{pmatrix} = \begin{bmatrix} \cos(2\pi p) & \dfrac{L}{2\pi n_0 p}\sin(2\pi p) \\ -\dfrac{2\pi n_0 p}{L}\sin(2\pi p) & \cos(2\pi p) \end{bmatrix} \begin{pmatrix} r_1 \\ \dfrac{dr_1}{dz} \end{pmatrix}$$

Phase change caused by a waveplate:

$$\phi = 2\pi(n_2 - n_1)z/\lambda$$

Grating equation:

$$d(\sin\theta + \sin\alpha_m) = m\lambda \text{ or } \alpha_m = \sin^{-1}\left[\frac{m\lambda}{d} - \sin\theta\right]$$

FTIR transmission equation:

$$T = 1 - |(z^2 + \delta^2)^2[(z^2 - \delta^2)^2 + 4z^2\delta^2 \coth^2\beta]^{-1}|$$

Propagation constant:

$$\beta = (2\pi d/\lambda)(n^2\sin^2\theta - 1)^{1/2}$$

z for polarization perpendicular to the plane of incidence:

$$z = 1/(n\cos\theta) \text{ and } \delta = -(n^2\sin^2\theta - 1)^{-1/2}$$

Equation Summary

z for polarization parallel to the plane of incidence:

$$z = (\cos\theta)/n \text{ and } \delta = (n^2 \sin^2\theta - 1)^{1/2}$$

Optical power vs fluid level height:

$$P(h) = 1 - 3.5 \times 10^{-3} h + 1.5 \times 10^{-5} h^2 - 3.3 \times 10^{-5} h^3$$

Optimum deformer spacing:

$$\Lambda = \frac{2\pi a n_0}{NA}$$

s-polarized power reflection coefficient:

$$R_s = \left| \frac{n_1 \cos\theta_1 - n_2 \sqrt{1 - \left[\left(\frac{n_1}{n_2}\right)\sin\theta_1\right]^2}}{n_1 \cos\theta_1 + n_2 \sqrt{1 - \left[\left(\frac{n_1}{n_2}\right)\sin\theta_1\right]^2}} \right|^2$$

p-polarized power reflection coefficient:

$$R_p = \left| \frac{n_1 \sqrt{1 - \left[\left(\frac{n_1}{n_2}\right)\sin\theta_1\right]^2} - n_2 \cos\theta_1}{n_1 \sqrt{1 - \left[\left(\frac{n_1}{n_2}\right)\sin\theta_1\right]^2} + n_2 \cos\theta_1} \right|^2$$

Fractional transmission as a function of axial displacement:

$$T_A = \frac{2}{\pi}\cos^{-1}\left(\frac{d}{2a}\right) - \left(\frac{d}{\pi a}\right)\left[1 - \left(\frac{d}{2a}\right)^2\right]^{1/2}$$

Fractional transmission as a function of longitudinal displacement:

$$T_L = \left[\frac{1}{1 + \left(\frac{s}{a}\right)\tan\theta_c}\right]^2$$

Equation Summary

Transmission through two lossless polarizers:

$$I = \frac{1}{2} I_0 \cos^2\theta$$

Polarization-based rotation sensor response function:

$$I = \frac{1}{2} I_0 \alpha \left[1 - \cos\frac{\theta}{4}\right] \Leftrightarrow \theta = 4\cos^{-1}\left(1 - \frac{2I}{\alpha I_0}\right)$$

Photoelastic stress sensor response function:

$$I = \frac{I_0}{4}\left[1 - \cos\left(\frac{2\pi d\sigma}{f_\sigma}\right)\right]$$

Grating equation for equal angles of incidence and diffraction:

$$2d \sin\theta_0 = \lambda$$

First-order diffraction equation for q rotation:

$$2d \sin\left(\theta_0 + \frac{\theta}{8}\right) = \lambda \quad \text{or} \quad \theta = 8\left[\sin^{-1}\left(\frac{\lambda}{2d}\right) - \theta_0\right]$$

Optimum parameters for grating rotation sensor:

$$d = \frac{\lambda_1}{2\sin\frac{\pi}{8}} \quad \text{and} \quad \lambda_2 = \lambda_1 \frac{\sin\frac{3\pi}{8}}{\sin\frac{\pi}{8}}$$

Basic chirped grating response function:

$$x = \frac{\lambda - d_0}{d_0(\sin\theta_{in} + \sin\theta_{diff})}$$

Chirped grating linear displacement sensor response function:

$$x = \frac{\lambda - d_0}{2d_1 \sin\theta_{in}}$$

Equation Summary

Fluorescence decay time vs absolute temperature:

$$\tau = \frac{1 + e^{(-\Delta E/k_B T)}}{R_E + R_T e^{(-\Delta E/k_B T)}}$$

Planck's radiation law:

$$F(\lambda) = \frac{2\pi hc^2}{\lambda^5 (e^{hc/k_B \lambda T} - 1)}$$

Wein's law:

$$\lambda_p = 2900/T$$

Phase delay in Mach–Zehnder and Michelson interferometers:

$$\phi = \frac{2\pi nL}{\lambda} = 2\pi\kappa$$

Change in phase in the Mach–Zehnder and Michelson interferometers:

$$d\phi = \frac{dL}{L} + \frac{dn}{n} + \frac{d\kappa}{\kappa}$$

Phase dither associated with Mach–Zehnder and Michelson interferometers:

$$\phi_{dither} = \Delta F \sin(\omega t)(L_1 + L_2)\frac{n}{c}$$

Open loop fiber optic gyro (rotation sensor):

$$Z_R = \frac{2\Omega RL}{\lambda c}$$

Closed-loop fiber optic gyro (rotation sensor):

$$F = \frac{2R\Omega}{\lambda n}$$

Response of a Sagnac acoustic sensor with half of the Sagnac loop shielded:

$$R(P(t)) = \left[\frac{ABnL^2}{4c}\right]\omega\sin(\omega t)$$

Equation Summary

Sagnac strain sensor response:

$$\frac{dF}{F} = -\left(\frac{dL}{L}\right)$$

Bragg fiber grating temperature response:

$$\frac{d\lambda}{\lambda} = (\alpha + \zeta)\Delta T$$

Bragg fiber grating longitudinal strain response:

$$\frac{d\lambda}{\lambda} = (1 - p_e)\varepsilon$$

Finesse of Fabry–Pérot sensor:

$$F = \frac{4R}{(1-R)^2}$$

Optical frequency domain reflectometry:

$$f_D = \frac{2nL\dfrac{d\lambda}{dt}}{\lambda^2}$$

Frequency division multiplexing:

$$F_m = (L - L_m)\frac{n}{c}$$

Phase noise in Mach–Zehnder and Michelson interferometers:

$$d\phi = 2\pi(dF)(L_1 - L_m)\frac{n}{c}$$

Brillouin sensor frequency shifts:

$$\upsilon_B = 2n\frac{v_a}{\lambda_p}$$

Lock-in amplifier output:

$$V = A\langle V_S V_R\rangle_{dc}$$

Bibliography

M. Beck and T. Hirschfeld, "Apparatus including optical fiber for fluorescence immunoassay," US Patent #4,582,809 (April 15, 1986).

M. A. Belkerdid, N. Ghandeharioun, and B. Brennan, "Fiber optic fluid level sensor," *Proc. SPIE* **566**, 153–158 (1986) [doi: 10.1117/12.949781].

J. W. Berthold et al., "Design and Characterization of a High Temperature Fiber-Optic Pressure Transducer," *J. Lightwave Technol.* **5**(7), 870 (1987).

T. Bosselmann et al., "Fiber optic temperature sensor using fluorescence decay time," *Proc. SPIE* **514**, 151 (1984) [doi: 10.1117/12.945072].

W. K. Burns, ed., *Optical Fiber Rotation Sensing*, Academic Press, Boston (1994).

B. A. Childers et al., "Fiber optic position and shape sensing device and method relating thereto," US Patent Application Publication 2007/0065077 (2007).

R. Claus and R. S. Rogowski, eds., *Fiber Optic Smart Structures and Skins V*, *Proc. SPIE* **1798** (1992).

B. Culshaw and J. Dakin, eds., *Optical Fibre Sensors*, Vols. I, II, III, and IV, Artech House, Boston (1988–1996).

R. R. Dils, "Optical Fiber Thermometer," US Patent #4,576,486 (May 18, 1986).

H. H. Du, G. Pickrell, E. Udd, C. S. Baldwin, J. J. Benterou, and A. Wang, eds., *Fiber Optic Sensors and Applications XI*, *Proc. SPIE* **9098** (2014).

R. DePaula and J. Berthold, eds., *Fiber Optic and Laser Sensors XIV*, *Proc. SPIE* **2839** (1996).

B. Glisic and D. Inaudi, *Fibre Optic Methods for Structural Monitoring*, John Wiley & Sons, New York (2007).

M. C. Hutley, *Diffraction Gratings*, Academic Press, London (1982).

Bibliography

A. D. Kersey, "A Review of Recent Developments in Fiber Optic Sensor Technology," *Opt. Fiber Technol.* **2** (3), 291–317 (1996).

R. H. Kingston, *Detection of Optical and Infrared Radiation*, Springer-Verlag, Berlin (1978).

G. Kirchhoff, "On the relation between the radiating and absorbing powers of different bodies for light and heat," *Annalen der Physik* **109**, 275 (1860).

C. D. Kissinger, "Fiber optic proximity probe," US Patent #3,327,584 (June 27, 1967).

R. D. LaClair, W. B. Spillman, Jr., and W. W. Kuhns, "Long stroke optical fiber linear position sensor for the FLASH program," *Proc. SPIE* **2840**, 137–141 (1996) [doi: 10.1117/12.254223].

N. Lagakos et al., "Microbend fiber-optic sensor," *Appl. Opt.* **26**(11), 2171 (1987).

W. R. Lawrence, "Fiber optic transducer and method," US Patent #4,358,678 (November 9, 1982).

J. N. Liu et al., "Development of a porous polymer pH optrode," *Opt. Lett.* **17**(24), 1815 (1992).

J. M. López-Higuera, ed., *Handbook of Optical Fibre Sensing Technology*, John Wiley & Sons, New York (2002).

J. M. López-Higuera, J. Jones, M. Lopez-Amo, and J. L. Santos, eds., *Int. Conf. Opt. Fibre Sensors*, Proceedings of SPIE (1998–2014).

A. Mendez and T. F. Morse, *Specialty Optical Fibers Handbook*, Academic Press, Amsterdam (2007).

J. H. Porter, "Differential Fiber Optic Differential Pressure Sensor," US Patent #4,210,029 (July 1, 1980).

B. E. A. Saleh and M. C. Teich, *Fundamentals of Photonics*, John Wiley & Sons, New York (1991).

Bibliography

G. B. Scott and D. E. Lacklison, "Magnetooptic Properties and Applications of Bismuth Substituted Iron Garnets," *IEEE Trans. Magnetics* **12**(4), 292 (1976).

W. B. Spillman, Jr., "Multimode fiber-optic hydrophone based on a Schlieren technique," *Appl. Opt.* **20**(3), 465 (1981).

W. B. Spillman, Jr., "The evolution of smart structures/materials," Proc. 1st European Conf. Smart Structures and Materials, p. 97, CRC Press (1992).

W. B. Spillman, Jr. and D. H. McMahon, "Frustrated-total-internal-reflection multimode fiber-optic hydrophone," *Appl. Opt.* **19**(1), 113–117 (1980).

W. B. Spillman, Jr. and D. H. McMahon, "Multimode fiber optic hydrophone based on the photoelastic effect," *Appl. Opt.* **21**(19), 3511 (1982).

W. B. Spillman, Jr. and D. H. McMahon, "Multimode fiber optic sensors based on the photoelastic effect," *Proc. SPIE* **412**, 110–114 (1983) [doi: 10.1117/12.935803].

W. B. Spillman, Jr. and R. E. Rudd, "Enhanced performance Faraday sensor," *Proc. SPIE* **2070**, 294–304 (1993) [doi: 10.1117/12.169910].

W. B. Spillman, Jr., D. R. Patriquin, and D. H. Crowne, "Fiber optic linear displacement sensor based upon a variable period diffraction grating," *Appl. Opt.* **28**(17), 3550 (1989).

W. B. Spillman, Jr. et al., "A 'smart' bed for non-intrusive monitoring of patient physiological factors," *J. Meas. Sci. Technol.* **15**(8), 1614 (2004).

W. B. Spillman, Jr. et al., "Statistical mode sensor for fiber optic vibration sensing applications," *Appl. Opt.* **28**(15), 3166 (1989).

P. S. Theocaris and E. E. Gdoutos, *Matrix Theory of Photoelasticity*, Springer-Verlag, Berlin (1979).

E. Udd, "An overview of fiber optic sensors," *Rev. Sci. Instruments* **66**(8), 4015 (1995).

Bibliography

E. Udd, "Fiber optic smart structures," *Proc. IEEE* **84**(6), 884–894 (1996).

E. Udd, ed., *Fiber Optic Smart Structures,* John Wiley & Sons, New York (1995).

E. Udd and W. B. Spillman, Jr., *Fiber Optic Sensors: an Introduction for Engineers and Scientists,* 2nd Ed., John Wiley & Sons, Hoboken, NJ (2011).

C. A. Villarruel et al., "Evanescent wave fiber optic chemical sensor," *Proc. SPIE* **798**, 225–229 (1987) [doi: 10.1117/12.941110].

J. D. Weiss, "Fiber Optic Sensor Employing Successively Destroyed Coupled Points or Reflectors for Detecting Shock Wave Speed and Damage Location," US Patent #5,446,278 (August 29, 1995).

A. Yariv, *Introduction to Optical Electronics,* 2nd Ed., Holt, Rinehart and Winston, New York (1976).

S. Yin, P. B. Ruffin, and F. T. S Yu, *Fiber Optic Sensors*, 2nd Ed., CRC Press, Boca Raton, FL (2008).

Index

Index

Index

Index

William B. Spillman, Jr., is a retired Associate Professor of Physics at Virginia Tech. He received his A.B. in Math-Physics from Brown University in 1968 and his M.S. and Ph.D. in Physics from Northeastern University in 1972 and 1977, respectively. Prior to his academic career, he worked as a scientist, research manager, and director of research for Sperry Corp., Geo-Centers, Inc., Hercules, Inc., and the Goodrich Corp., among others. He is the co-author/editor of 7 books and more than 180 technical publications. He also holds 46 US patents. In 1997, he was elected a Fellow of SPIE, and in 2000 he received a SPIE recognition award for his society activities in smart structures and materials. He was elected a Fellow and Chartered Physicist in 2001 and a Chartered Scientist in 2004 by the Institute of Physics in the UK. In February 2006, he received a Lifetime Achievement Award from SPIE for his research and professional activities in smart materials and structures. He has been active in the field of fiber optic sensing since its inception, with numerous publications and patents.

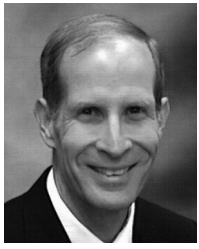

Eric Udd is President of Columbia Gorge Research, a company he founded to promote fiber optic sensor technology and its applications. He has been involved in the field of fiber optic sensors since 1977, with fundamental contributions to fiber rotation, acceleration, acoustic, pressure, vibration, strain, temperature, humidity and corrosion sensors. At McDonnell Douglas (1977–1993), he managed over 30 government and commercial programs on fiber optic sensors that resulted in products used on the 777 and other commercial aircraft, launch vehicles, and spacecraft. In 1993, Udd founded Blue Road Research, working on civil structures, oil and gas projects, aerospace, and defense. In January 2006, he began full-time work at Columbia Gorge Research and developed new applications in the electric power and medical fields, as well as aerospace and defense.

Udd has 48 issued US Patents, with additional applications pending. He has written over 150 papers, chaired more than 30 international conferences on fiber sensors, edited textbooks, and contributed many book chapters. He is a McDonnell Douglas Fellow, an SPIE Fellow, and an OSA Fellow. He was awarded the David Richardson Medal by OSA in 2009 for his work on fiber optic sensors and the field of fiber optic smart structures.

Fiber Optic Sensors

William B. Spillman, Jr.
Eric Udd

The continued improvement and reduction in costs associated with fiber optic technology associated with fiber sensors permit application areas that were previously inaccessible. These trends are expected to continue as new techniques become available and older ones are successfully adapted to new applications. This Field Guide provides a broad introduction to a variety of fiber optic sensors that have been successfully developed from the 1970s to the present. A wide range of examples are provided to inspire readers with ideas for new sensors and uses.

SPIE Field Guides

The aim of each *SPIE Field Guide* is to distill a major field of optical science or technology into a handy desk or briefcase reference that provides basic, essential information about optical principles, techniques, or phenomena.

Written for you—the practicing engineer or scientist—each field guide includes the key definitions, equations, illustrations, application examples, design considerations, methods, and tips that you need in the lab and in the field.

John E. Greivenkamp
Series Editor

SPIE.
P.O. Box 10
Bellingham, WA 98227-0010
ISBN: 9781628413342
SPIE Vol. No.: FG34

www.spie.org/press/fieldguides